IEEE Access
Multidisciplinary | Rapid Review | Open Access Journal

Received 23 August 2023, accepted 17 September 2023, date of publication 22 September 2023,
date of current version 28 September 2023.

Digital Object Identifier 10.1109/ACCESS.2023.3318476

RESEARCH ARTICLE

Information Extraction Using Spectral Analysis of the Chattering of the Smooth Variable Structure Filter

AHSAN SAEEDZADEH[1], PEYMAN SETOODEH[1], (Senior Member, IEEE), MARJAN ALAVI[2], (Senior Member, IEEE), AND SAEID HABIBI[1], (Member, IEEE)
[1]Department of Mechanical Engineering, McMaster University, Hamilton, ON L8S 4L8, Canada
[2]W Booth School of Engineering Practice and Technology, Hamilton, ON L8S 4L8, Canada

Corresponding author: Ahsan Saeedzadeh (Saeedzaa@mcmaster.ca)

This work was supported by the Natural Sciences and Engineering Research Council of Canada (NSERC) under Grant RGPIN-2020-05735.

ABSTRACT Smooth variable Structure Filter (SVSF) is a model-based robust nonlinear filtering technique, based on the variable structure concept formulated in a predictor-corrector form. It is used for estimating the states of a system and is robust against noise and modeling uncertainties. It ensures stability in the face of model mismatch resulting from a poor model or fault, at the expense of corrective actions, which cause chattering. The chattering contains mismatch footprints that can be exploited to identify system faults and determine their severity. In this paper, information extraction from chattering is investigated to identify model mismatch based on the spectral contents of the chattering signal. To verify the effectiveness of the developed framework for chattering analysis, two case studies are considered. First, the power spectrum of the chattering signal has been employed to identify mismatch and the potential of recovering the temporal information of the model mismatch from the spectrogram is studied, using Short Time Fourier Transform (STFT) for an underdamped second-order system. Then, the proposed strategy is applied to detect and measure the severity of leakage and friction faults as well as the bulk modulus mismatch in an electro-hydraulic actuator.

INDEX TERMS Fault detection, information extraction, smooth variable structure filter, spectral analysis, STFT.

I. INTRODUCTION

Estimation is a process to obtain the states or parameters of interest using partial, noisy, and inaccurate measurements. It can be applied in areas such as tracking, control, system identification, statistical inference, signal processing, system monitoring, and fault management [1]. Kalman Filter (KF) is the best-known optimal state estimation strategy that minimizes the mean square error of the estimation for a stochastic linear system with zero-mean Gaussian noise. To overcome the requirement of linearity, gaussian noise distribution, and a fairly known model, different versions of KF such as the Extended Kalman Filter (EKF) and the Unscented Kalman Filter (UKF) have been proposed [2]. Later, a more computationally demanding recursive Bayesian estimator was proposed referred to as Particle Filter (PF) [3], also known as the sequential Monte Carlo method [4]. Particle Filters are applicable to general nonlinear systems with non-Gaussian Probability Density Functions (PDFs), but their performance is determined by the number of particles, which reflects the computational demand. Conceptually, when the number of particles approaches infinity, the estimation error for a particle filter will converge to zero [5].

State estimation is the cornerstone of model-based Fault Detection and Diagnosis (FDD) strategies, be it online or offline. Model-based FDD methods involve the development of a system model through either a fundamental comprehension of the system's underlying physics or system identification. This model serves as a benchmark to create mathematical links between inputs and measurements and

The associate editor coordinating the review of this manuscript and approving it for publication was Min Wang.

generate residuals that contain fault signatures using the concept of analytical redundancy. These residuals are then processed through a decision-making tool for diagnostic purposes. The benefit of this approach compared to data-driven methods lies in the meaningful interpretation of each physical state and parameter of the model, which significantly enhances the diagnostic process. The major model-based FDD approaches proposed in literature [6] can be classified into observer-based methods like full-state observers [7], [8] and unknown input observers [9], [10], parity relation [11], [12], [13], [14], optimization-based [15], [16], [17], stochastic filter-based methods like Kalman filters [18], [19], [20] and SVSF [21], [22], adaptive multiple model estimation [23], [24], [25], [26], [27], and parameter estimation [28], [29], [30], [31]. Isolability and robustness (especially for online FDD) play an important role in the FDD process. Adaptive multiple model estimation can resolve the isolability problem, where perfect decoupling of estimation error residual is not possible, or the parameter estimation problem is not observable [32]. Fault or any other source of uncertainty will cause a model mismatch. Therefore, the robustness of the estimation is an important property of FDD problems.

The KF becomes sub-optimal and potentially unstable when the model used is not matching the real system [33]. The same problem exists in other Bayesian filters such as UKF and PF, designed under the assumption that the system model is largely known [34]. The numerical instability of the KF, due to round-off error, can be resolved with square root forms such as the Cholesky and UD factorizations [kaminski1971discrete, bierman2006factorization], or using a larger process noise [5]. Variable Structure Filter (VSF) is a robust estimation method based on the sliding mode concept, in a predictor-corrector form [35]. The Smooth Variable Structure Filter (SVSF) is an extension of VSF, applicable to non-linear systems. Using SVSF, it is desired that the estimated state trajectory converges to an existence subspace around the ground truth and remains within this subspace. A large a priori error due to model mismatch or fault condition leads to chattering. SVSF uses a smoothing boundary layer to eliminate the chattering typical to sliding mode concept. If the smoothing boundary is larger than the width of the existence subspace, the estimated state trajectory will be smoothened, and chattering will not occur [36]. An optimal version of the SVSF has been proposed for linear systems and uses a Variable Boundary Layer (VBL) to minimize the estimation error for zero-mean Gaussian additive noise [37]. However, when it comes to FDD, choosing the smoothing boundary layer is a delicate matter. On one hand, model mismatch or fault condition may lead to chattering by reducing the effectiveness of the smoothing boundary layer [33]. Therefore, the chattering signal can be used as an indication of model mismatch or fault. On the other hand, increasing the width of the smoothing boundary layer smoothens the estimated state trajectory, which in turn, increases the chance of missing a fault by the deployed FDD algorithm.

This paper proposes a framework for model mismatch identification and fault detection based on the information content of the chattering signal obtained from the SVSF algorithm. The proposed framework relies on spectral analysis of the chattering in the estimated state trajectory. To verify the effectiveness of the proposed strategy, it is applied to a linear stochastic dynamic system as well as an Electro-Hydraulic Actuator (EHA). It is shown that typical fault conditions seen in hydraulic systems involving bulk modulus mismatch, leakage, and friction faults can be identified using the chattering signal of the SVSF. Contributions of the paper can be summarized as follows:

- Exploration of the novel concept of utilizing chattering signals of the SVSF for fault diagnosis.
- Information extraction from spectral analysis of the chattering using the probability distribution of the chattering power spectrum.
- Examination of the ability to capture fault-related temporal details from chattering spectrogram using short-time Fourier transform.
- Implementation of the developed approach to detect and measure the severity of leakage and friction faults as well as the bulk modulus mismatch within an electro-hydraulic actuator.

The organization of this paper is as follows. In section II, the chattering signal of the smooth variable structure filter is defined while briefly outlining the filtering strategy. The development of the chattering equation based on model mismatch, process noise, and measurement noise is covered in Section III. The section considers the information content in chattering for systems with both full and partial state measurements. In a case study for a second-order system, the potential of applying the chattering equation to derive information about model mismatch is then demonstrated. Section IV focuses on spectral analysis of the chattering signal using the Fast Fourier Transform (FFT) and spectrogram. The proposed approach is applied to an EHA system to detect bulk modulus, leakage, and friction faults in section V. Concluding remarks are provided in section VI.

II. THE CHATTERING SIGNAL OF THE SMOOTH VARIABLE STRUCTURE FILTER

Consider a general linear stochastic dynamic system with zero-mean Gaussian process and measurement noise denoted by $\mathbf{v}(k)$ and $\mathbf{w}(k)$, which are characterized by the covariance matrices $\mathbf{Q}(k)$ and $\mathbf{R}(k)$, respectively.

$$\mathbf{x}(k+1) = \mathbf{A}\mathbf{x}(k) + \mathbf{B}\mathbf{u} + \mathbf{v}(k), \tag{1}$$

$$\mathbf{z}(k) = \mathbf{C}\mathbf{x}(k) + \mathbf{w}(k). \tag{2}$$

Assuming the modeling uncertainties to be $\Delta\mathbf{A}(k)$, $\Delta\mathbf{B}(k)$, and $\Delta\mathbf{C}(k)$ as follows:

$$\Delta\mathbf{A}(k) = \mathbf{A} - \hat{\mathbf{A}},$$

$$\Delta\mathbf{B}(k) = \mathbf{B} - \hat{\mathbf{B}},$$
$$\Delta\mathbf{C}(k) = \mathbf{C} - \hat{\mathbf{C}}, \tag{3}$$

where $\hat{\mathbf{A}}$, $\hat{\mathbf{B}}$, and $\hat{\mathbf{C}}$ contain the nominal parameters of the model. The SVSF then iteratively repeats the following four steps to estimate the states of the system [36].

1) The states are predicted according to the system model and a priori estimates are obtained.

$$\hat{\mathbf{x}}(k+1|k) = \hat{\mathbf{A}}\hat{\mathbf{x}}(k|k) + \hat{\mathbf{B}}\hat{\mathbf{u}}(k|k), \tag{4}$$
$$\hat{\mathbf{z}}(k+1|k) = \hat{\mathbf{C}}\hat{\mathbf{x}}(k+1|k). \tag{5}$$

2) A priori and a posterior output error estimates are obtained.

$$\mathbf{e_z}(k+1|1) = \mathbf{z}(k+1) - \hat{\mathbf{z}}(k+1|k), \tag{6}$$
$$\mathbf{e_z}(k|k) = \mathbf{z}(k) - \hat{\mathbf{z}}(k|k). \tag{7}$$

3) The corrective term is calculated.
   - If measurements are available for all states:

$$\mathbf{K}(k+1) = \hat{\mathbf{C}}^{-1}\left(|\mathbf{e_z}(k+1|k)| + \gamma\,|\mathbf{e_z}(k|k)|\right) \odot \text{sat}\left(\mathbf{e_z}(k+1|k), \Psi\right), \tag{8}$$

     where γ is the convergence rate, Ψ is the smoothing boundary layer, $\odot$ is the Schur product, and sat$(\cdot, \Psi)$ stands for saturation function.
   - If measurements are not available for some states but the system is observable, then the corrective term will be calculated based on Luenberger's reduced-order observer. For states with associated measurements, the corrective term is the same as above.

$$\mathbf{K_u}(k+1) = \hat{\mathbf{C}}_1^{-1}\left(|\mathbf{e_z}(k+1|k)| + \gamma\,|\mathbf{e_z}(k|k)|\right) \odot \text{sat}\left(\mathbf{e_z}(k+1|k), \Psi\right), \tag{9}$$

$$\mathbf{K_l}(k+1) = \left(\left|\hat{\Phi}_{22}\hat{\Phi}_{12}^{-1}\mathbf{e_z}(k+1|k)\right| + \gamma\left|\hat{\Phi}_{12}^{-1}\mathbf{e_z}(k|k)\right|\right) \odot \text{sat}\left(\hat{\Phi}_{22}\hat{\Phi}_{12}^{-1}\mathbf{e_z}(k+1|k), \Psi\right), \tag{10}$$

$$\mathbf{K}(k+1) = \begin{bmatrix}\mathbf{K_u}(k+1)\\ \mathbf{K_l}(k+1)\end{bmatrix}. \tag{11}$$

   Assuming the system has n states and m outputs, the measurement matrix will have two blocks: $\mathbf{C} = \begin{bmatrix}\mathbf{C}_1 & \mathbf{C}_2\end{bmatrix}$, where $\mathbf{C}_1$ is a full rank $m \times m$ matrix associated with measured states and $\mathbf{C}_1$ is an $m \times (n-m)$ matrix corresponding to the unmeasured states. Subscript u is used for state vectors directly linked to measurements, while subscript l refers to the states without corresponding measurements. Matrix $\hat{\Phi} = \mathbf{T}^{-1}\hat{\mathbf{A}}\mathbf{T} = \begin{bmatrix}\hat{\Phi}_{11} & \hat{\Phi}_{12}\\ \hat{\Phi}_{21} & \hat{\Phi}_{22}\end{bmatrix}$ is calculated using transformation T, which rearranges the state vector based on the mentioned two subsets of states [36].

4) The a posteriori state estimate is then updated by refining the a priori estimate using the corrective term.

$$\hat{\mathbf{x}}(k+1|k+1) = \hat{\mathbf{x}}(k+1|k) + \mathbf{K}(k+1). \tag{12}$$

The chattering occurs when a priori estimation error is larger than the boundary layer as shown below:

$$Chattering_i(k) = \begin{cases} 0, & \text{if } |e_i(k|k-1)| < \Psi_i \\ (|e_i(k|k-1)| - \Psi_i) & \\ \text{sgn}(e_i(k|k-1)), & \text{otherwise} \end{cases} \tag{13}$$

where $Chattering_i(k)$ denotes the chattering, $e_i(k|k-1)$ is the a priori estimation error, and Ψ_i is the smoothing boundary layer for state i. To avoid chattering under the normal condition, the smoothing boundary layer should be larger than the upper bound of the uncertain dynamics associated with the a priori state estimate ($\boldsymbol{\beta}$). This upper bound is obtained based on system uncertainties and noise as [36]:

$$\boldsymbol{\beta} = \sup\Big(\mathbf{C}\left(\Delta\mathbf{A}\left(\mathbf{C}^{-1}\mathbf{z}(k) - \mathbf{w}(k)\right)\right) + \Delta\mathbf{B}\mathbf{u}(k) + \mathbf{v}(k)) + \mathbf{w}(k+1)\Big). \tag{14}$$

For an observable system with fewer measurements, states should be transformed, then $\boldsymbol{\beta}$ can be calculated as explained in [36].

$$\begin{bmatrix}\mathbf{d}_1(k)\\ \mathbf{d}_2(k)\end{bmatrix} = \Delta\Phi\begin{bmatrix}\mathbf{z}(k)\\ \mathbf{y}(k)\end{bmatrix} + \Delta\mathbf{G}\mathbf{u}(k) + \begin{bmatrix}\bar{\mathbf{v}}_1(k)\\ \bar{\mathbf{v}}_2(k)\end{bmatrix}, \tag{15}$$

$$\boldsymbol{\beta} = \max\left((\mathbf{I}-\gamma)^{-1}\left|\hat{\Phi}_{22}\right|, \gamma^{-1}\left|\hat{\Phi}_{22}\right|, \gamma^{-1}, \mathbf{I}\right) \times \sup\left(\left|\mathbf{d}_2(k) - \hat{\Phi}_{22}\hat{\Phi}_{12}^{-1}\mathbf{d}_1(k)\right| + \left|\hat{\Phi}_{12}^{-1}\mathbf{d}_1(k-1)\right|\right). \tag{16}$$

The existence boundary can be determined based on an upper bound on $\mathbf{d}(k)$ due to uncertain dynamics, $\Phi = \mathbf{T}^{-1}\mathbf{A}\mathbf{T} = \begin{bmatrix}\Phi_{11} & \Phi_{12}\\ \Phi_{21} & \Phi_{22}\end{bmatrix}$, $\mathbf{G} = \mathbf{T}^{-1}\mathbf{B}$, and $\begin{bmatrix}\bar{\mathbf{v}}_1(k)\\ \bar{\mathbf{v}}_2(k)\end{bmatrix} = \mathbf{T}^{-1}\mathbf{v}(k) - \begin{bmatrix}\Phi_{11}\\ \Phi_{22}\end{bmatrix}\mathbf{w}(k+1)$.

To avoid chattering, Ψ should be larger than $\boldsymbol{\beta}$. However, choosing a very large smoothing boundary layer ($\psi_i \gg \beta_i$ for all i) reduces the robustness of the filter. The SVSF estimation inside the smoothing boundary layer can be improved by finding an optimal variable boundary layer [37].

To detect fault conditions from the chattering effect in the SVSF (or SVSF-VBL), the upper bound on the smoothing boundary layer should be chosen based on system uncertainties (Fig.1a). As shown in Fig.1c, when the smoothing boundary layer is smaller than, chattering occurs even during normal system conditions. On the other hand, as shown in Fig.1b, if the smoothing boundary layer is larger than $\boldsymbol{\beta}$, fault cannot be detected. Assuming that matrix $\mathbf{C}$ is exactly known, the existence boundary layer obtained from (14) can be considered as an approximate value for the smoothing boundary layer [36].

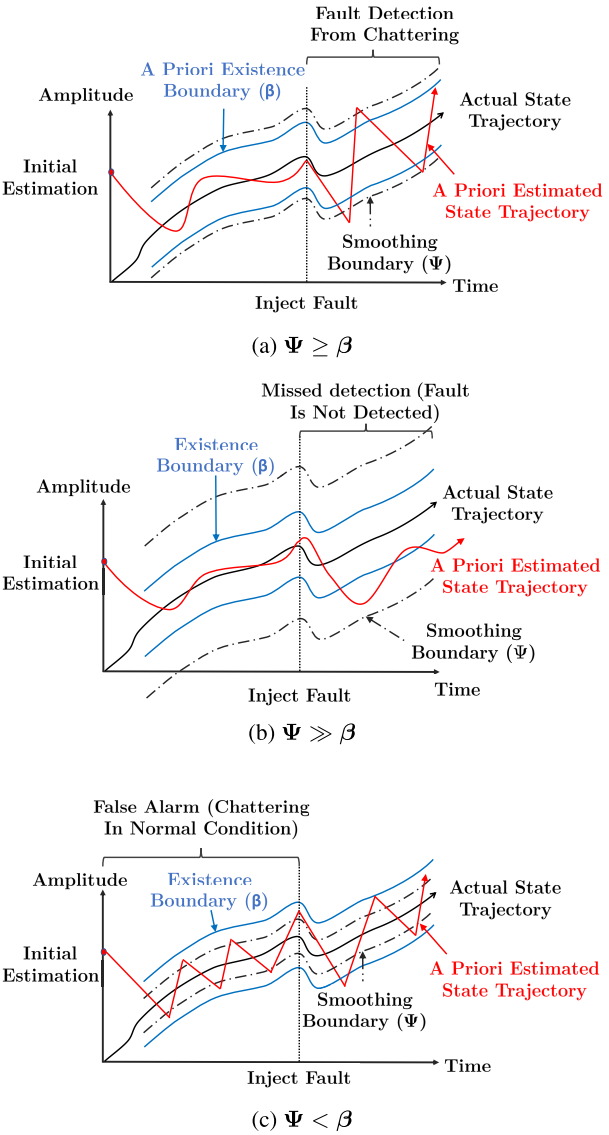

FIGURE 1. Fault detection from chattering signal of SVSF for different relative values of existence and smoothing boundary layers.

III. INFORMATION EXTRACTION FROM CHATTERING SIGNAL

When a model mismatch or fault is detected from the chattering signal of the SVSF-VBL, an auxiliary filter is run in parallel to extract information from the chattering signal. This auxiliary filter is a variant of the mentioned SVSF that has the same recursive steps with one exception. In (8), (9), and (10), the saturation function, sat$(\cdot, \Psi)$, is replaced with the sign function, sgn$(\cdot)$. In other words, the auxiliary filter does not use any smoothing boundary layer.

A. CHATTERING SIGNAL FOR FULL MEASUREMENT OF THE STATE VARIABLES

According to (13), the chattering for the auxiliary filter that uses the sign function is equal to the a priori error:

$$\begin{aligned}\textbf{chattering}(k+1) &= \mathbf{e_z}(k+1|k)\\ &= \mathbf{z}(k+1) - \hat{\mathbf{z}}(k+1|k)\\ &= \mathbf{z}(k+1) - \hat{\mathbf{C}}\hat{\mathbf{x}}(k+1|k). \end{aligned} \tag{17}$$

Substituting (4) and (2) into (17) yields:

$$\begin{aligned}\textbf{chattering}(k+1) &= \mathbf{C}\mathbf{x}(k+1) + \mathbf{w}(k+1)\\ &\quad - \hat{\mathbf{C}}\left(\hat{\mathbf{A}}\hat{\mathbf{x}}(k|k) + \hat{\mathbf{B}}\mathbf{u}(k)\right). \end{aligned} \tag{18}$$

Substituting the states from (1) gives:

$$\begin{aligned}\textbf{chattering}(k+1) &= \mathbf{C}\mathbf{A}\mathbf{x}(k) + \mathbf{C}\mathbf{B}\mathbf{u}(k) + \mathbf{C}\mathbf{v}(k)\\ &\quad + \mathbf{w}(k+1) - \hat{\mathbf{C}}\left(\hat{\mathbf{A}}\hat{\mathbf{x}}(k|k) + \hat{\mathbf{B}}\mathbf{u}(k)\right). \end{aligned} \tag{19}$$

The a posteriori state estimate obtained by the auxiliary filter is calculated as follows:

$$\begin{aligned}\hat{\mathbf{z}}(k|k) &= \hat{\mathbf{x}}(k|k-1) + \mathbf{K}(k) = \hat{\mathbf{x}}(k|k-1)\\ &\quad + \hat{\mathbf{C}}^{-1}\left(|\mathbf{e_z}(k|k-1)| + \gamma\,|\mathbf{e_z}(k-1|k-1)|\right)\\ &\quad \odot \operatorname{sgn}\left(\mathbf{e_z}(k|k-1)\right) = \hat{\mathbf{x}}(k|k-1)\\ &\quad + \hat{\mathbf{C}}^{-1}\left(\mathbf{e_z}(k-1|k) + \gamma\,|\mathbf{e_z}(k-1|k-1)|\right.\\ &\quad \left.\odot \operatorname{sgn}\left(\mathbf{e_z}(k|k-1)\right)\right), \end{aligned} \tag{20}$$

where the estimation error decays with rate γ [36].

$$\begin{aligned}|\mathbf{e_z}(k-1|k-1)| &= \gamma\,|\mathbf{e_z}(k-2|k-2)|\\ &= \gamma^{k-1}\,|\mathbf{e_z}(0|0)|. \end{aligned} \tag{21}$$

Substituting (21) into (20) and further simplifying it using (6), (5), and (2) yields:

$$\begin{aligned}\hat{\mathbf{x}}(k|k) &= \hat{\mathbf{x}}(k|k-1) + \hat{\mathbf{C}}^{-1}\left(\mathbf{z}(k) - \hat{\mathbf{z}}(k|k-1)\right)\\ &\quad \times \hat{\mathbf{C}}^{-1}\gamma^{k-1}\,|\mathbf{e_z}(0|0)| \odot \operatorname{sgn}\left(\mathbf{e_z}(k|k-1)\right)\\ &= \hat{\mathbf{C}}^{-1}\mathbf{z}(k) + \gamma^{k-1}\,|\mathbf{e_z}(0|0)| \odot \operatorname{sgn}\left(\mathbf{e_z}(k|k-1)\right)\\ &= \hat{\mathbf{C}}^{-1}\mathbf{C}\mathbf{x}(k) + \hat{\mathbf{C}}^{-1}\mathbf{w}(k) + \gamma^{k-1}\,|\mathbf{e_z}(0|0)|\\ &\quad \odot \operatorname{sgn}\left(\mathbf{e_z}(k|k-1)\right). \end{aligned} \tag{22}$$

By substituting (22) into (19) and rearranging it, the chattering can be formulated as a function of model mismatch and system noise:

$$\begin{aligned}\textbf{chattering}(k+1) &= \left(\mathbf{C}\mathbf{A} - \hat{\mathbf{C}}\hat{\mathbf{A}}\hat{\mathbf{C}}^{-1}\mathbf{C}\right)\mathbf{x}(k)\\ &\quad + \left(\mathbf{C}\mathbf{B} - \hat{\mathbf{C}}\hat{\mathbf{B}}\right)\mathbf{u}(k) + \mathbf{C}\mathbf{v}(k)\\ &\quad - \hat{\mathbf{C}}\hat{\mathbf{A}}\hat{\mathbf{C}}^{-1}\mathbf{w}(k) + \mathbf{w}(k+1)\\ &\quad + \hat{\mathbf{C}}\hat{\mathbf{A}}\hat{\mathbf{C}}^{-1}\gamma^{k-1}\,|\mathbf{e_z}(0|0)|\\ &\quad \odot \operatorname{sgn}\left(\mathbf{e_z}(k|k-1)\right). \end{aligned} \tag{23}$$

B. CHATTERING SIGNAL FOR FEWER MEASUREMENTS THAN STATE VARIABLES

For an observable system, the chattering of the state estimates of the auxiliary filter can be obtained based on Luenberger's reduced order observer [36]. Applying

Luenberger's transformation, equation (19) can be written as follows:

$$\begin{aligned}\mathbf{chattering_u}(k+1) &= \mathbf{C}_1\Phi\mathbf{T}\mathbf{x}(k) - \hat{\mathbf{C}}_1\hat{\Phi}\mathbf{T}\hat{\mathbf{x}}(k|k) \\ &\quad + \left(\mathbf{C}_1\mathbf{G} - \hat{\mathbf{C}}_1\hat{\mathbf{G}}\right)\mathbf{u}(k) + \bar{\mathbf{v}}_1(k),\end{aligned} \tag{24}$$

where subscript "**u**" refers to the states that are measured. The a posteriori state estimate can be obtained from (9), (10), and (11) as in (25), shown at the bottom of the next page. Then, the chattering can be obtained by substituting (25) into (24) as shown in (26), at the bottom of the next page.

Ignoring the impact of the initial error, assuming $\hat{\mathbf{C}}_1 = \mathbf{C}_1$ and $\mathbf{T}$ being identity, which can be achieved by rearranging the states, equation (26) can be simplified as follows:

$$\begin{aligned}&\mathbf{chattering_u}(k+1) \\ &= \mathbf{C}_1\Delta\Phi\mathbf{x}(k) + \mathbf{C}_1\Delta\mathbf{G}\mathbf{u}(k) + \bar{\mathbf{v}}_1(k) \\ &\quad - \hat{\mathbf{C}}_1\begin{bmatrix}\hat{\Phi}_{12}\hat{\Phi}_{22}\hat{\Phi}_{12}^{-1}\mathbf{d}_1(k-1) + \hat{\Phi}_{12}\mathbf{d}_2(k-1) \\ \hat{\Phi}_{22}^2\hat{\Phi}_{12}^{-1}\mathbf{d}_1(k-1) + \hat{\Phi}_{22}\mathbf{d}_2(k-1)\end{bmatrix}.\end{aligned} \tag{27}$$

The chattering of the states without an associated measurement can be obtained based on the chattering of the measured states, using Luenberger's transformation [36]:

$$\begin{aligned}\mathbf{chattering_l}(k+1) &= \hat{\Phi}_{22}\hat{\Phi}_{12}^{-1}\mathbf{chattering_u}(k+1) \\ &\quad - \hat{\Phi}_{22}\hat{\Phi}_{12}^{-1}\mathbf{d}_1(k) + \mathbf{d}_2(k),\end{aligned} \tag{28}$$

where subscript "**l**" refers to the states without an associated measurement.

The modified upper bound of the uncertain dynamics associated with the a priori state estimate can be calculated from the following equation:

$$\boldsymbol{\beta}_{estimated} = \sup\left(\mathbf{chattering}(k)\right). \tag{29}$$

To avoid chattering, the smoothing boundary layer (Ψ) should be larger than $\boldsymbol{\beta}_{estimated}$.

C. MODEL MISMATCH DETECTION FROM CHATTERING SIGNAL OF THE SVSF

In this section, the model mismatch detection for a second-order system from the chattering signal of the SVSF is investigated. The discretized state-space model of a general second-order system with damping ratio ζ, natural frequency ω_0, measurement noise $w(k)$, and process noise $v_1(k)$ and $v_2(k)$ is given in (30), assuming only the first state has been measured.

$$\begin{aligned}&\begin{cases}x_1(k+1) = x_1(k) + T_s x_2(k) + v_1(k) \\ x_2(k+1) = -T_s\omega_0^2 x_1(k) + (1 - 2T_s\zeta\omega_0)\,x_2(k) \\ \qquad\qquad +T_s bu(k) + v_2(k)\end{cases} \\ &z(k) = x_1(k) + w(k)\end{aligned} \tag{30}$$

where T_s denotes the time-step and u is the system input. Under the normal condition let us assume an undamped ($\zeta = 0$) system with $\omega_0 = 2$Hz, $b = 100$, uncorrelated process noise $v_1(k) \sim \mathcal{N}\left(0, 10^{-10}\right)$ and $v_2(k) \sim \mathcal{N}\left(0, 10^{-8}\right)$, measurement noise $w(k) \sim \mathcal{N}\left(0, 10^{-8}\right)$, and $T_s = 0.001$s. For the estimated parameters being equal to the normal condition, model matrices are obtained as follows:

$$\begin{aligned}&\hat{\mathbf{A}} = \mathbf{A} = \begin{bmatrix}1 & 0.001 \\ -0.0125 & 1\end{bmatrix}, \quad \hat{\mathbf{B}} = \mathbf{B} = \begin{bmatrix}0 \\ 0.1\end{bmatrix}, \\ &\hat{\mathbf{C}} = \mathbf{C} = \begin{bmatrix}0 & 1\end{bmatrix}.\end{aligned} \tag{31}$$

If the smoothing boundary layer is chosen to be larger than the SVSF chattering under normal conditions, then chattering in the SVSF indicates a model mismatch. For state x_1, which is directly measured, the width of the smoothing boundary layer can be calculated by substituting (31) and (27) into (29). Ignoring the effect of the initial error, we obtain:

$$\begin{aligned}\psi_1 \geq \beta_{1,estimated} = \sup\Big(&\bar{\mathbf{v}}_1(k) - \hat{\Phi}_{12}\hat{\Phi}_{22}\hat{\Phi}_{12}^{-1}\mathbf{d}_1(k-1) \\ &+ \hat{\Phi}_{12}\mathbf{d}_2(k-1)\Big)\end{aligned} \tag{32}$$

Let us denote the argument of the supremum function in the above equation by δ_1. Substituting the numerical values of the parameters, we have:

$$\begin{aligned}\delta_1 &= v_1(k) - v_1(k-1) - 0.001v_2(k-1) - w(k) \\ &\quad + \left(1 - 1.25\times10^{-5}\right)w(k-1)\end{aligned} \tag{33}$$

Considering that the measurement noise and process noise are independent and white, the distribution of δ_1 is obtained as:

$$\begin{aligned}\delta_1 \sim \mathcal{N}\Big(&\mu_{v_1(k)} - \mu_{v_1(k-1)} - 0.001\mu_{v_2(k-1)} - \mu_{w(k)} \\ &+ \mu_{w(k-1)}, \sigma^2_{v_1(k)} + \sigma^2_{v_1(k-1)} + 10^{-6}\sigma^2_{v_2(k)} \\ &+ \sigma^2_{w(k)} + \sigma^2_{w(k-1)}\Big) \approx \mathcal{N}\left(0, 2.02\times10^{-8}\right)\end{aligned} \tag{34}$$

Since δ_1 has a zero-mean normal distribution if the assigned value to the smoothing boundary layer is between $3\sigma_{\delta_1(k)}$ and $4\sigma_{\delta_1(k)}$, then chattering will occur with a probability of 0.2% to 0.01%. Therefore, it would not be necessary to consider a larger smoothing boundary layer. As mentioned previously, choosing a large smoothing boundary layer suppresses the chattering in effect, therefore, decreases the sensitivity for model mismatch detection. This increases the chance of missing faults. On the other hand, choosing a small boundary layer increases the probability of chattering occurrence even under normal conditions. This will lead to false alarms. Hence, the smoothing boundary layer must be chosen based on a trade-off between reducing the probability of missing faults and reducing the probability of false alarms. Choosing $\psi_1 = 5\times10^{-4} \approx 3.5\sigma_{\delta_1(k)}$, the probability of the chattering is calculated as follows according to the normal distribution table:

$$\Pr\left(\psi_1 < \beta_{1,estimated}\right) = \Pr\left(5\times10^{-4} < |\delta_1(k)|\right) \approx 0.067 \tag{35}$$

This means that chattering is almost impossible during normal operation and any chattering reflects a fault or model mismatch in the system. For the unmeasured state x_2, the smoothing boundary is obtained by substituting (32), (28), and (21) into (29):

$$\begin{aligned}\psi_2 &\geq \beta_{2,estimated} \\ &= \sup\Big(1000\Big(\bar{\mathbf{v}}_1(k) \\ &\quad - \hat{\Phi}_{12}\hat{\Phi}_{22}\hat{\Phi}_{12}^{-1}\mathbf{d}_1(k-1) + \hat{\Phi}_{12}\mathbf{d}_2(k-1)\Big) \\ &\quad - 1000v_1(k) + 1000w(k) + v_2(k) - 12.5w(k)\Big). \end{aligned} \tag{36}$$

Similarly, denoting the argument of the supremum function in the above equation by δ_1, the distribution of δ_2 is calculated as:

$$\delta_2(k) \sim \mathcal{N}\left(0, 3.0135 \times 10^{-2}\right). \tag{37}$$

The sensitivity of the chattering signal to fault or model mismatch depends on the smoothing boundary layer, which is determined by process and measurement noise. A higher noise level needs a larger smoothing boundary layer, which will overshadow the fault or model mismatch. Comparing (34) with (37), δ_1 has a sharper distribution than δ_2 due to its lower variance, which reflects a lower level of uncertainty. This is rational because x_2 is not measured directly. Therefore, the chattering signal of the measured state x_1 is used to detect the model mismatch here.

The state-space model of the second-order system described in (30) includes two parameters: damping ratio and natural frequency. Hence, in this case, model mismatch refers to any difference between the values of these two parameters in the system whose states are estimated and the model of this system, which is used by the filter that estimates the states. To evaluate the capability of the proposed model mismatch detection method based on the chattering signal of the SVSF, the following scenario is considered for creating a model mismatch. While the model used by SVSF remains unchanged, for the system whose states are estimated, during the time interval [1s, 2s], the natural frequency is changed from 2Hz to 3Hz, and during the time interval [3s, 4s], the damping ratio is changed from zero to 0.1. Three different smoothing boundary layers are selected for the measured state based on δ_1, while keeping the smoothing boundary layer of the unmeasured state the same for comparison. As shown in Fig.2, when the smoothing boundary layer is too large ($\psi_1 = 0.002 \gg \sigma_{\delta_1(k)}$), chattering does not occur. Since the chattering signal is used as a secondary indicator along with the innovation vector as the primary indicator of model mismatch, in the absence of chattering in this case, there is not any extra information that can be used for detecting model mismatch. Conversely, when the smoothing boundary layer is too small ($\psi_1 = 0.0001 < \sigma_{\delta_1(k)}$), chattering occurs even under normal conditions, and again analysis of the chattering signal is not helpful for model-mismatch detection. Hence, the value of ψ_1 must be selected carefully. This figure also shows that the estimation error increases when there is a model mismatch in the system. It is more severe for x_2, which

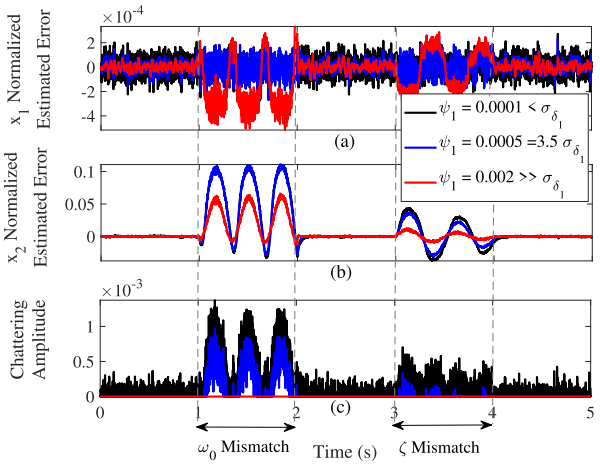

FIGURE 2. Model mismatch detection from chattering signal of SVSF for a second order system. Normalized estimation error for (a) measured and (b) unmeasured states. (c) Chattering signal of the measured state for three different smoothing boundary values. For a small smoothing boundary layer (black), chattering occurs even during normal conditions. For a large smoothing boundary layer (red), chattering does not occur when there is model mismatch. Only for a medium smoothing boundary layer (blue), chattering signal is helpful for model-mismatch-detection.

$$\begin{aligned}\hat{\mathbf{x}}(k|k) &= \hat{\mathbf{x}}(k|k-1) + \begin{bmatrix}\mathbf{K_u}(k)\\ \mathbf{K_l}(k)\end{bmatrix} \\ &= \begin{bmatrix}\hat{\mathbf{x_u}}(k|k-1) + \hat{\mathbf{C}}_1^{-1}\left(\mathbf{z}(k) - \hat{\mathbf{z}}(k|k-1)\right) + \hat{\mathbf{C}}_1^{-1}\gamma^{k-1}\left|\mathbf{e_z}(0|0)\right| \odot \operatorname{sgn}\left(\mathbf{e_z}(k|k-1)\right)\\ \hat{\mathbf{x}}_\mathbf{l}(k|k-1) + \hat{\Phi}_{22}\hat{\Phi}_{12}^{-1}\left(\mathbf{z}(k) - \hat{\mathbf{z}}(k|k-1)\right) + \gamma^{k-1}\left|\hat{\Phi}_{12}^{-1}\mathbf{e_z}(0|0)\right| \odot \operatorname{sgn}\left(\hat{\Phi}_{12}^{-1}\mathbf{e_z}(k|k-1)\right)\end{bmatrix} \\ &= \begin{bmatrix}\hat{\mathbf{C}}_1^{-1}\mathbf{C}_1\mathbf{x_u}(k) + \hat{\mathbf{C}}_1^{-1}\gamma^{k-1}\left|\mathbf{e_z}(0|0)\right| \odot \operatorname{sgn}\left(\mathbf{e_z}(k|k-1)\right)\\ \hat{\mathbf{x}}_\mathbf{l}(k) + \hat{\Phi}_{22}\hat{\Phi}_{12}^{-1}\mathbf{d}_1(k-1) + \mathbf{d}_2(k-1) + \gamma^{k-1}\left|\hat{\Phi}_{12}^{-1}\mathbf{e_z}(0|0)\right| \odot \operatorname{sgn}\left(\hat{\Phi}_{12}^{-1}\mathbf{e_z}(k|k-1)\right)\end{bmatrix}, \end{aligned} \tag{25}$$

$$\begin{aligned}\mathbf{chattering_u}(k+1) &= \mathbf{C}_1\Phi\mathbf{T}\mathbf{x}(k) + \left(\mathbf{C}_1\mathbf{G} - \hat{\mathbf{C}}_1\hat{\mathbf{G}}\right)\mathbf{u}(k) + \bar{\mathbf{v}}_1(k) - \hat{\mathbf{C}}_1\hat{\Phi}\mathbf{T} \\ &\quad \begin{bmatrix}\hat{\mathbf{C}}_1^{-1}\mathbf{C}_1\mathbf{x_u}(k) + \hat{\mathbf{C}}_1^{-1}\gamma^{k-1}\left|\mathbf{e_z}(0|0)\right| \odot \operatorname{sgn}\left(\mathbf{e_z}(k|k-1)\right)\\ \hat{\mathbf{x}}_\mathbf{l}(k) + \hat{\Phi}_{22}\hat{\Phi}_{12}^{-1}\mathbf{d}_1(k-1) + \mathbf{d}_2(k-1) + \gamma^{k-1}\left|\hat{\Phi}_{12}^{-1}\mathbf{e_z}(0|0)\right| \odot \operatorname{sgn}\left(\hat{\Phi}_{12}^{-1}\mathbf{e_z}(k|k-1)\right)\end{bmatrix}. \end{aligned} \tag{26}$$

is not measured directly and relies more on a correct model. This error is larger for a smaller boundary layer because it means that SVSF has more confidence in the model, which is not correct anymore.

IV. SPECTRAL ANALYSIS OF THE CHATTERING SIGNAL

In state estimation, it is not straightforward to distinguish between noise and model mismatch based on their effects on the innovation vector. Deploying SVSF for state estimation, the corresponding chattering signals provide a secondary set of indicators that can be used for model-mismatch detection. To extract information from the chattering signal, an auxiliary SVSF without a smoothing boundary layer is used. As indicated in (23), (27), and (28), the chattering signal contains information about the severity of mismatch between the state-space model used by the SVSF and the dynamics of the actual system whose states are estimated by the filter. Spectral analysis provides a powerful tool for extracting this information from the noisy chattering signal using strategies such as Fast Fourier Transform (FFT) and Short-Time Fourier Transform (STFT). In this regard, looking at the spectrogram of the chattering signal will be very revealing. Spectrogram represents the frequency content of the chattering signal as it varies over time. Hence, it provides clues on occurrence of events such as faults that change the system and lead to model mismatch. Power spectrum is defined as the squared modulus of the Fourier transform. For a random signal, the power spectrum will similarly exhibit randomness. In certain contexts, when studying random signals, the expected power spectrum (or the expected value of squared modulus of the Fourier transform) is simply referred to as the power spectrum. In this study, the power spectrum shown by $\mathcal{S}$, is a random variable, and when needed, we explicitly denote the expected power spectrum using the notation $\mathbb{E}[\mathcal{S}]$. Sources of randomness in the system dynamics are process noise and measurement noise, which are zero-mean white Gaussian processes. To lay the groundwork for deriving mathematical expressions for power spectrum of the chattering signal, first, Lemma 1 presents the probability distribution of the real and imaginary parts of the discrete Fourier transform coefficients for zero-mean white Gaussian processes, emphasizing the orthogonality of these real and imaginary parts. Building on the results of Lemma 1, Lemma 2 expresses that the power spectrum of a stationary zero-mean white Gaussian noise at each frequency follows a chi-squared distribution. The result of Lemma 2 is then used to find the distribution of the power spectrum of the chattering signal. This distribution is needed to calculate the confidence interval for model mismatch detection.

Lemma 1: The discrete Fourier transform coefficients of a stationary zero-mean white Gaussian noise, $v(k) \sim \mathcal{N}\left(0, \sigma^2\right)$, with N samples are independent and zero-mean white Gaussian with the variance of $\frac{N\sigma^2}{2}$.

$$\Re\left\{V^{(N)}(\omega_n)\right\} \sim \mathcal{N}\left(0, \frac{N\sigma^2}{2}\right),$$
$$\Im\left\{V^{(N)}(\omega_n)\right\} \sim \mathcal{N}\left(0, \frac{N\sigma^2}{2}\right),$$
$$\Re\left\{V^{(N)}(\omega_n)\right\} \perp \Im\left\{V^{(N)}(\omega_n)\right\}, \tag{38}$$

for $\omega_n = \frac{2\pi}{N}n$, where $-\lfloor\frac{N-1}{2}\rfloor \leq n \leq \lfloor\frac{N}{2}\rfloor$. $V^{(N)}(\omega_n)$ is the discrete Fourier transform of the noise signal v at n^{th} frequency, $\Re$ and $\Im$ denote real and imaginary parts respectively, and $\lfloor x \rfloor$ denotes the floor function (the largest integer, which is less than or equal to x).

Proof: Let us define the normalized $V^{(N)}(\omega_n)$ as follows:

$$\widetilde{V}^{(N)}(\omega_n) = \frac{1}{\sqrt{2\pi N}} V^{(N)}(\omega_n) = \frac{1}{\sqrt{2\pi N}} \sum_{i=1}^{n} v(k) e^{-i\omega_n k}. \tag{39}$$

According to [38], $\widetilde{V}^{(N)}(\omega_n)$ is a zero-mean complex Gaussian random variable with the following distribution:

$$\widetilde{V}^{(N)}(\omega_n) \sim \mathcal{N}_c\left(0, f(\omega_n)\right), \tag{40}$$

where f is the spectral density function. For white noise, it is flat and equal to $\frac{\sigma^2}{2\pi}$. Since the family of normal distributions is closed under linear transformation, the distribution of $V^{(N)}(\omega_n)$ can be obtained from (40) as:

$$V^{(N)}(\omega_n) \sim \mathcal{N}_c\left(0, 2\pi N f(\omega_n)\right) \Rightarrow V^{(N)}(\omega_n) \sim \mathcal{N}_c\left(0, N\sigma^2\right) \tag{41}$$

Real and imaginary parts are obtained as a direct consequence of (41):

$$\mathcal{N}_c\left(0, N\sigma^2\right) \Leftrightarrow \begin{cases} \Re\left\{V^{(N)}(\omega_n)\right\} & \sim \mathcal{N}\left(0, \frac{N\sigma^2}{2}\right) \\ \Im\left\{V^{(N)}(\omega_n)\right\} & \sim \mathcal{N}\left(0, \frac{N\sigma^2}{2}\right) \\ \Re\left\{V^{(N)}(\omega_n)\right\} & \perp \Im\left\{V^{(N)}(\omega_n)\right\} \end{cases} \tag{42}$$

□

Lemma 2: The power spectrum of a stationary zero-mean white Gaussian noise, $v(k) \sim \mathcal{N}\left(0, \sigma^2\right)$, with N evenly spaced samples, follows a central chi-squared distribution of order 2 with the expected value of σ^2:

$$\frac{2\mathcal{S}_n^{(N)}(\omega_n)}{\sigma^2} \sim \chi_2^2 \quad \text{and} \quad \mathbb{E}\left[\mathcal{S}_n^{(N)}(\omega_n)\right] = \sigma^2,$$
$$\text{for} \quad \omega_n = \frac{2\pi}{N}n,$$
$$\text{where:} \quad 0 \leq n \leq \lfloor\frac{N}{2}\rfloor - 1, \tag{43}$$

where $\mathcal{S}_n^{(N)}(\omega_n)$ is the power spectrum of noise signal v at n^{th} frequency.

Proof: Based on the power spectrum definition, the following equation holds:

$$\mathcal{S}_n^{(N)}(\omega_n) = \frac{1}{N}\left|V_n^{(N)}(\omega_n)\right|^2$$

$$= \frac{1}{N}\left(\Re\left\{V^{(N)}(\omega_n)\right\}^2 + \Im\left\{V^{(N)}(\omega_n)\right\}^2\right) \quad (44)$$

The following is valid because the family of normal distributions is closed under the linear transformation:

$$\Re\left\{V^{(N)}(\omega_n)\right\} \sim \mathcal{N}\left(0, \frac{N\sigma^2}{2}\right)$$
$$\Rightarrow \frac{\sqrt{2}\Re\left\{V^{(N)}(\omega_n)\right\}}{\sigma\sqrt{N}} \sim \mathcal{N}(0,1), \quad (45)$$
$$\Im\left\{V^{(N)}(\omega_n)\right\} \sim \mathcal{N}\left(0, \frac{N\sigma^2}{2}\right)$$
$$\Rightarrow \frac{\sqrt{2}\Im\left\{V^{(N)}(\omega_n)\right\}}{\sigma\sqrt{N}} \sim \mathcal{N}(0,1), \quad (46)$$

Knowing that $\Re\left\{V^{(N)}(\omega_n)\right\} \perp \Im\left\{V^{(N)}(\omega_n)\right\}$ from *lemma* 1, definition of chi-squared distribution yields:

$$\frac{2\Re\left\{V^{(N)}(\omega_n)\right\}^2}{N\sigma^2} + \frac{2\Im\left\{V^{(N)}(\omega_n)\right\}^2}{N\sigma^2} \sim \chi_2^2$$
$$\Rightarrow \frac{2}{\sigma^2}\left(\frac{1}{N}\left(\Re\left\{V^{(N)}(\omega_n)\right\}^2 + \Im\left\{V^{(N)}(\omega_n)\right\}^2\right)\right) \sim \chi_2^2$$
$$\Rightarrow \frac{2\mathcal{S}_n^{(N)}(\omega_n)}{\sigma^2} \sim \chi_2^2. \quad (47)$$

Knowing that the expected value of central chi-squared distribution is equal to the degrees of freedom, the expected value of the power spectrum is obtained as:

$$\mathbb{E}\left[\frac{2\mathcal{S}_n^{(N)}(\omega_n)}{\sigma^2}\right] = 2 \Rightarrow \mathbb{E}\left[\mathcal{S}_n^{(N)}(\omega_n)\right] = \sigma^2. \quad (48)$$

□

The power spectrum of the chattering signal for each frequency is defined as follows:

$$\mathcal{S}_{\mathbf{chattering}}{}^{N}(\omega_n) = \frac{1}{N}\left|\mathcal{F}\left(\mathbf{chattering}_k\right)_n\right|^{\odot 2}$$
$$= \frac{1}{N}\left|\sum_{k=1}^{N}\mathbf{chattering}(k)e^{-i\omega_n k}\right|^{\odot 2},$$
$$\text{for} \quad \omega_n = \frac{2\pi}{N}n,$$
$$\text{where:} \quad 0 \le n \le \lfloor\frac{N}{2}\rfloor - 1, \quad (49)$$

where, $\mathcal{S}_{chattering_i}$ is the power spectrum (only for half of the frequencies because it is symmetric) of the chattering signal of the state i at *nth* frequency, $\mathcal{F}$ denotes the discrete Fourier transform, N is the number of samples, $\mathbf{chattering}_k := \mathbf{chattering}(1), \mathbf{chattering}(2) \ldots \mathbf{chattering}(N)$ is a sequence of chattering vectors, $\odot$ is element-wise also known as Schur operation ($\mathbf{B} = \mathbf{A}^{\odot 2} \Rightarrow b_{ij} = a_{ij}^2$), t is signal duration, and T_s is sampling time. To obtain frequency in Hz, the following transformation is applied on ω_n:

$$\omega = F_s\omega_n \quad \text{where:} \quad \frac{1}{T_s}, \quad (50)$$

where, ω is the frequency in Hz and F_s is the sampling rate. As shown in (49) and (50) the resolution and upper bound of ω depend on the signal duration and sampling frequency, respectively. Hence, the sampling size, N, is a crucial parameter that affects the spectrogram. Hereafter, the superscript N is removed since it is considered that the number of samples is fixed. Substituting (23) into (49) and ignoring the impact of the initial error, the power spectrum of chattering signal is obtained as follows using the linearity property of the discrete Fourier transform:

$$\mathcal{S}_{\mathbf{chattering}}(\omega_n) = \frac{1}{N}\left|\left(\mathbf{CA} - \hat{\mathbf{C}}\hat{\mathbf{A}}\hat{\mathbf{C}}^{-1}\mathbf{C}\right)\mathcal{F}(\mathbf{x}_k)_n + \left(\mathbf{CB} - \hat{\mathbf{C}}\hat{\mathbf{B}}\right)\mathcal{F}(\mathbf{u}_k)_n + \mathbf{C}\mathcal{F}(\mathbf{v}_k)_n - \hat{\mathbf{C}}\hat{\mathbf{A}}\hat{\mathbf{C}}^{-1}\mathcal{F}(\mathbf{w}_k)_n + \mathcal{F}(\mathbf{w}_{k+1})_n\right|^{\odot 2}. \quad (51)$$

Under the normal condition with no model mismatch, equation (51) can be rewritten as:

$$\mathcal{S}_{\mathbf{chattering}}(\omega_n) = \frac{1}{N}\left|\mathbf{C}\mathcal{F}(\mathbf{v}_k)_n - \mathbf{C}\hat{\mathbf{O}}\hat{\mathbf{O}}^{-1}\mathcal{F}(\mathbf{w}_k)_n + \mathcal{F}(\mathbf{w}_{k+1})_n\right|^{\odot 2}. \quad (52)$$

Using the shift theorem for discrete Fourier transform, (52) is further simplified as:

$$\mathcal{S}_{\mathbf{chattering}}(\omega_n) = \frac{1}{N}\left|\mathbf{C}\mathcal{F}(\mathbf{v}_k)_n + \left(e^{i\omega_n}\mathbf{I} - \hat{\mathbf{C}}\hat{\mathbf{A}}\hat{\mathbf{C}}^{-1}\right)\mathcal{F}(\mathbf{w}_k)_n\right|^{\odot 2}. \quad (53)$$

Let us consider independent stationary white process and measurement noise with zero mean Gaussian distributions as:

$$\mathbf{Q}(k) = \mathbf{v}(k)\mathbf{v}(k)^{\mathsf{T}} = \text{diag}\left(\boldsymbol{\sigma}_{\mathbf{v}}{}^2\right), \quad (54)$$
$$\mathbf{R}(k) = \mathbf{w}(k)\mathbf{w}(k)^{\mathsf{T}} = \text{diag}\left(\boldsymbol{\sigma}_{\mathbf{w}}{}^2\right), \quad (55)$$

where, $\mathbf{Q}(k)$ and $\mathbf{R}(k)$ are the covariance matrices of the process and measurement noise respectively, $\boldsymbol{\sigma}^2_{\mathbf{v}_i}$ is the variance of the process noise for state i, and $\boldsymbol{\sigma}^2_{\mathbf{w}_j}$ is the variance of measurement noise for measurement j.

Regarding the predictor-corrector form of the SVSF, at each time instant, chattering depends on measurement noise for both prediction, $\mathbf{w}(k-1)$, and correction, $\mathbf{w}(k)$. Therefore, as shown in (53), the chattering signal exhibits autocorrelation due to the implicit accumulation of the effect of delayed measurement noise terms over time. The expected value of the power spectrum of the chattering signal is obtained using *lemmas* 1 and 2 (all the cross-correlation terms become zero due to independence and zero mean condition of discrete Fourier transform from *lemma* 1):

$$\mathbb{E}\left[\mathcal{S}_{\mathbf{chattering}}(\omega_n)\right] = \mathbf{C}^{\odot 2}\mathbb{E}\left[\frac{1}{N}\left|\mathcal{F}(\mathbf{v}_k)_n\right|^{\odot 2}\right] + \left|e^{i\omega_n}\mathbf{I} - \hat{\mathbf{C}}\hat{\mathbf{A}}\hat{\mathbf{C}}^{-1}\right|^{\odot 2}\mathbb{E}\left[\frac{1}{N}\left|\mathcal{F}(\mathbf{w}_k)_n\right|^{\odot 2}\right]$$

$$= \mathbf{C}^{\odot 2}\mathbb{E}\left[\mathcal{S}_{\mathbf{v}}\right] + \left|e^{i\omega_n}\mathbf{I} - \hat{\mathbf{C}}\hat{\mathbf{A}}\hat{\mathbf{C}}^{-1}\right|^{\odot 2}\mathbb{E}\left[\mathcal{S}_{\mathbf{w}}\right]$$
$$= \mathbf{C}^{\odot 2}\boldsymbol{\sigma}_{\mathbf{v}}{}^2 + \left|e^{i\omega_n}\mathbf{I} - \hat{\mathbf{C}}\hat{\mathbf{A}}\hat{\mathbf{C}}^{-1}\right|^{\odot 2}\boldsymbol{\sigma}_{\mathbf{w}}{}^2. \quad (56)$$

Due to the exponential term in equation (56), which depends on frequency, it can be concluded that in general, the expected value of the power spectrum of the chattering signal is not flat under normal conditions (Fig.4).

A. FIND THE THRESHOLD FOR SPECTRAL DENSITY OF THE CHATTERING SIGNAL UNDER NORMAL CONDITION

To identify model mismatch, a threshold must be determined for the spectral density of the chattering signal that reflects normal conditions. This threshold should be intelligently specified in a way to decrease the chance of missing any model mismatch while avoiding false alarms. According to (52), there is an element of randomness in the power spectrum of the chattering signal. Therefore, the threshold should be obtained by taking account of the probability distribution of the power spectrum of the chattering signal, using a confidence interval. To be more precise, the following equation must hold to ensure that the probability of a false alarm is smaller or equal to $\alpha\%$:

$$\Pr\left(\mathcal{S}_{chattering_i} > threhold_i | Normal\ Condition\right) \leq \alpha\% \quad (57)$$

where $\mathcal{S}_{chattering_i}$ is the power spectrum of the chattering signal for measured state i, and $threshold_i$ is its corresponding threshold. Let us define the matrices $\mathbf{M}$ and Λ as follows:

$$\mathbf{M} := -\hat{\mathbf{C}}\hat{\mathbf{A}}\hat{\mathbf{C}}^{-1},$$
$$\lambda_{ij} := \begin{cases} m_{ij} & \text{for } i \neq j, \\ m_{ij}+1 & \text{for } i = j \text{ and } m_{ij} \geq 0, \\ m_{ij}-1 & \text{for } i = j \text{ and } m_{ij} < 0. \end{cases} \quad (58)$$

Given that $-1 \leq e^{i\omega_n} \leq 1$, the above definition leads to $\Gamma > \left(e^{i\omega_n}\mathbf{I} - \hat{\mathbf{C}}\hat{\mathbf{A}}\hat{\mathbf{C}}^{-1}\right)$. This inequality and (53) along with the independence of process and measurement noise, will lead to the following inequality:

$$\mathcal{S}_{\mathbf{chattering}}(\omega_n) \leq \frac{1}{N}\left|\mathbf{C}\mathcal{F}(\mathbf{v}_k)_n + \Gamma\mathcal{F}(\mathbf{w}_k)_n\right|^{\odot 2}. \quad (59)$$

Based on the linearity property of the DFT, equation (59) can be rewritten as:

$$\mathcal{S}_{\mathbf{chattering}}(\omega_n) \leq \frac{1}{N}\left|\mathcal{F}\left(\mathbf{C}\mathbf{v}_k + \Gamma\mathbf{w}_k\right)_n\right|^{\odot 2}. \quad (60)$$

Since $\mathbf{v}_k$ and $\mathbf{w}_k$ are mutually independent stationary white zero-mean Gaussian vectors, their linear combination is also a stationary white zero-mean Gaussian vector:

$$\Gamma_k = \mathbf{C}\mathbf{v}_k + \Gamma_{\mathbf{k}} \quad \text{where: } \Gamma_k \sim \mathcal{N}\left(0, \Sigma_\Gamma(k)\right)$$
$$\text{and } \Sigma_\Gamma(k) = \mathbf{C}\mathbf{Q}(k)\mathbf{C}^{\intercal} + \Gamma\mathbf{R}(k)\Gamma^{\intercal}. \quad (61)$$

Substituting (61) into (60), and using *lemma* 2, we have:

$$\mathcal{S}_{\mathbf{chattering}}(\omega_n) \leq \frac{1}{N}\left|\mathcal{F}\left(\Gamma_k\right)_n\right|^{\odot 2} = \mathcal{S}_\Gamma,$$

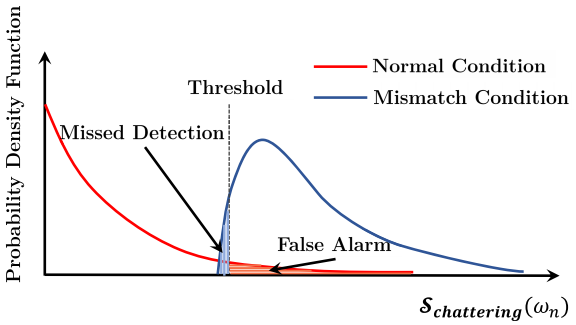

FIGURE 3. PDF of the chattering's power spectrum for normal and mismatched conditions.

$$\text{where: } \frac{2\mathcal{S}_{\Gamma_i}}{\Sigma_{\Gamma_{ii}}} \sim \chi^2_2. \quad (62)$$

where $\mathcal{S}_{\Gamma_i}$ is the power spectrum of the random signal associated with state i, which has a chi-squared distribution. Therefore, a threshold for the chattering signal under normal conditions will be obtained based on equation (57), using the chi-squared distribution table. When there is a model mismatch, a spike in the chattering power spectrum is expected according to the frequency content of the states and input signals as shown in (51). Higher peaks will result from a larger model mismatch, which can be used to evaluate the severity of the fault. If the chattering signal's power spectrum exceeds the threshold, it indicates a model mismatch in the system. Additionally, it is possible to acquire the frequency content of system states (such as natural frequencies) to be used for mismatch identification.

Since the threshold plays a key role in correctly detecting mismatch, it must be selected by taking account of system's measurement and process noise levels as well as the required confidence interval based on the probability distribution of the power spectrum of the chattering signal. Fig.3 conceptually illustrates how the threshold is chosen based on a trade-off between reducing the chance of missing model mismatches and avoiding false alarms regarding the PDF of the chattering's power spectrum for both normal and mismatch conditions. Under normal conditions, a higher level of noise leads to a heavier tail in the PDF, which in turn, increases the likelihood of missed detection and false alarm. However, a higher level of mismatch corresponds to a larger shift in the PDF, which makes detection easier. The same approach can be employed to analyze the chattering signal of the system with partial state measurement by substituting (26) and (28) into (49).

In the case study that follows, this approach is investigated for a second-order system.

B. MISMATCH IDENTIFICATION IN A SECOND-ORDER SYSTEM USING SPECTRAL ANALYSIS OF THE CHATTERING SIGNAL

Let us consider a second-order system as (30), with the natural frequency of $\omega_0 = 10Hz$, damping ratio $\zeta = 0.1$,

$b = 100$, and $T_s = 0.001s$. The process and measurement noise are assumed to be independent white zero-mean Gaussian with the following covariance matrices: $\mathbf{Q} = \text{diag}\left(10^{-8}, 10^{-6}\right)$, $\mathbf{R}_{low} = \text{diag}\left(10^{-8}, 10^{-6}\right)$, $\mathbf{R}_{high} = \text{diag}\left(10^{-6}, 10^{-4}\right)$.

In order to study the impact of noise level on mismatch identification, two levels of measurement noise are considered with one being 10 times higher than the other. Under normal conditions, system matrices are obtained as below:

$$\hat{\mathbf{A}} = \mathbf{A} = \begin{bmatrix} 1 & 0.001 \\ -3.1978 & 0.9887 \end{bmatrix}, \quad \hat{\mathbf{B}} = \mathbf{B} = \begin{bmatrix} 0 \\ 0.1 \end{bmatrix},$$
$$\hat{\mathbf{C}} = \mathbf{C} = \begin{bmatrix} 1 & 0 \\ 0 & 1 \end{bmatrix}. \tag{63}$$

A unit step is applied as the input, and system's behavior is observed for 4 seconds. Since $T_s = 0.001s$, simulation generates 4000 data points over 4 seconds. Fig.4 displays the power spectrum of the chattering signal for both states under normal conditions. As shown, the higher noise level requires a higher threshold. Higher measurement noise skews the power spectrum more, increasing the power density in high frequencies. The shift property in equation (53) is the cause of skewness. The power spectrum of the chattering signal remains below the threshold for the 0.1% false alarm level (99.9% confidence interval from chi-squared distribution), but for the 1% level, there are several false alarms in high frequencies, which is acceptable for 500 samples. To avoid false alarms completely, the number of samples (N) should be taken into account when selecting α. A conservative upper bound for the probability of false alarm in all frequencies is obtained as below:

$$\begin{aligned} &\Pr\Big(\left(\mathcal{S}_{chattering_i}(\omega_1) > thershold_i\right) \cup \cdots \cup \\ &\quad \left(\mathcal{S}_{chattering_i}(\omega_{\frac{N}{2}}) > thershold_i\right) | NormalCondition\Big) \\ &\leq \sum_{n=1}^{\frac{N}{2}} \Pr\Big(\mathcal{S}_{chattering_i}(\omega_n) > thershold_i | NormalCondition\Big) \\ &\leq \frac{N}{2}\alpha\%. \end{aligned} \tag{64}$$

In Fig.5, the power spectrum of the chattering signal for the second state, $chattering_2$, has been used to identify model mismatch. In this case, a very small change in natural frequency ($\omega_0 = 11Hz$ compared to $\omega_0 = 10Hz$ for normal conditions) is considered, while all other parameters remain unchanged. Accordingly, the state matrix of the system will change to $\mathbf{A} = \begin{bmatrix} 1 & 0.001 \\ -4.7769 & 0.9862 \end{bmatrix}$, while input and measurement matrices do not change ($\hat{\mathbf{B}} = \mathbf{B}$, $\hat{\mathbf{C}} = \mathbf{C}$). It can be seen from (23) or (51) that $chattering_1$ will not change when only ω_0 changes. Thus, the mismatch is not observable in $chattering_1$.

As shown, the mismatch causes a spike in the spectral density at 11Hz, which coincides with the natural frequency of the actual system. For the high measurement noise level shown in Fig.5, this peak is lower than the threshold, which means it cannot be separated from the noise effect. Using the expected power spectrum is one strategy to resolve this issue. For this purpose, using the idea of Monte Carlo simulation, average of the spectrogram is obtained for many realizations of the same event with the same input and identical conditions. Then, the averaged power spectrum of the noise will converge to the expected value, while the peak at 11Hz remains the same as demonstrated in Fig.6. Nevertheless, this approach cannot be used for real-time mismatch identification.

Fig.7 depicts the power spectrum of the chattering for different levels of mismatch, where the natural frequency of the real system is changed to $\omega_0 = 9Hz$, $12Hz$, and $15Hz$, as opposed to the nominal model with $\omega_0 = 10Hz$. Results demonstrate that the proposed approach is capable of separating various levels of mismatch and indicating the intensity of the mismatch based on the amplitude of the peak. As mentioned previously, the frequency resolution of the spectrogram depends on the duration of data gathering and the sampling rate.

C. EXTRACT TEMPORAL INFORMATION OF THE MISMATCH FROM THE SPECTROGRAM OF THE CHATTERING SIGNAL

Frequency content of the chattering signal changes when a mismatch or fault occurs in a system. Therefore, it would be beneficial for mismatch detection to extract temporal information about the frequency content of nonstationary signals. Time-varying spectrum, also known as the spectrogram, is a powerful tool to recover the temporal information along with the frequency content of the signal. Two well-known techniques can be deployed to generate the spectrogram: the Short-Time Fourier Transform (STFT) and the wavelet transform. The STFT method is used in this part to identify the mismatch from the chattering signal.

Let us assume the following scenario for the general second-order system presented in (30), where the process and measurement noise are independent white zero-mean Gaussian with $\mathbf{Q} = mathrmdiag\left(10^{-8}, 10^{-6}\right)$ and $\mathbf{R} = mathrmdiag\left(10^{-6}, 10^{-4}\right)$:

- Under normal conditions, the natural frequency of the system is 5Hz with no damping ratio.
- For the first 2 seconds, a model mismatch is introduced to the system by changing the natural frequency to 8Hz.
- Then, for 2 seconds system goes back to normal condition.
- Then again, for 2 seconds, a model mismatch is introduced, this time by changing the damping ratio to 0.1.
- Finally, the system becomes normal again until the end of the simulation.

According to the Heisenberg-Gabor limit, the periodical and temporal resolution of the spectrogram, which are both governed by the STFT window, have an inverse relationship.

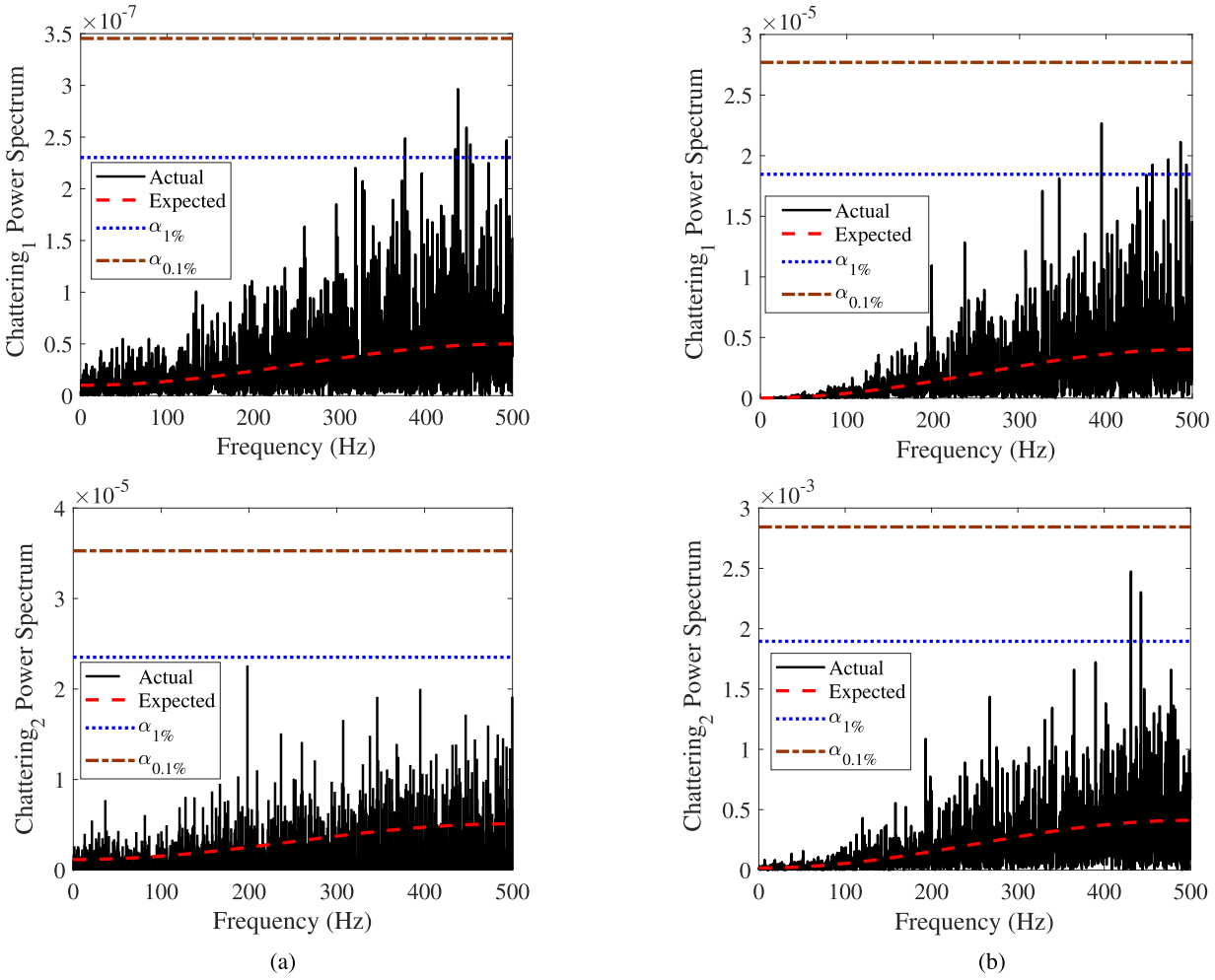

FIGURE 4. Power spectrum of the chattering signal under normal conditions for (a) low measurement noise level and (b) high measurement noise level, where α denotes the error probability.

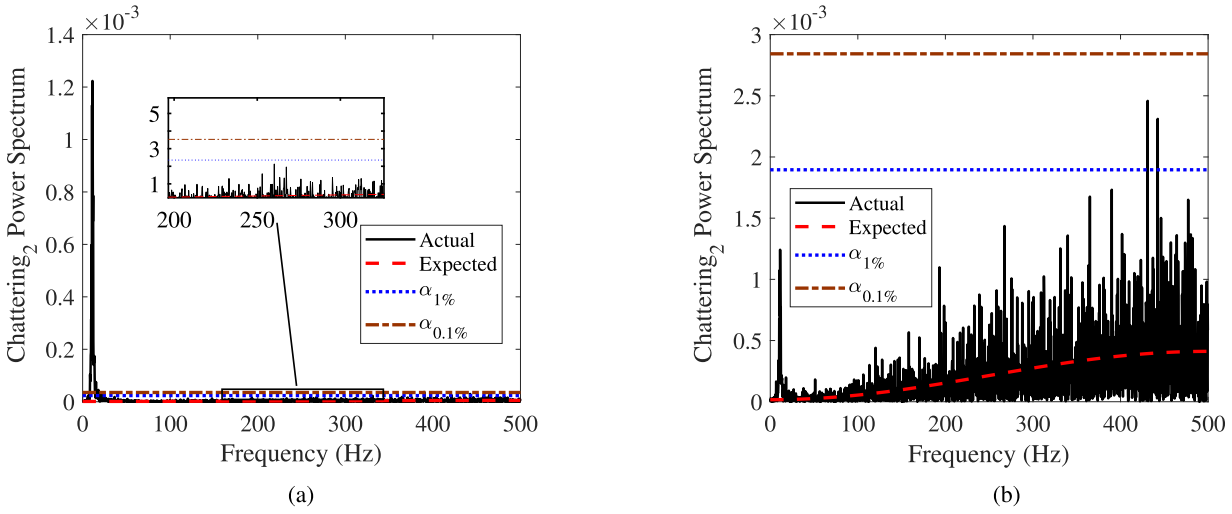

FIGURE 5. Power spectrum of the chattering signal with a mismatch ($\omega_0 = 11Hz$) for (a) low measurement noise level and (b) high measurement noise level, where α denotes the error probability.

A long window improves the frequency resolution but decreases the temporal resolution and vice versa. Therefore, the length of the window should be chosen carefully based on the application at hand. For this problem, the length of the window has been chosen to be one second, which gives a 1Hz frequency resolution and 1 second time resolution. The

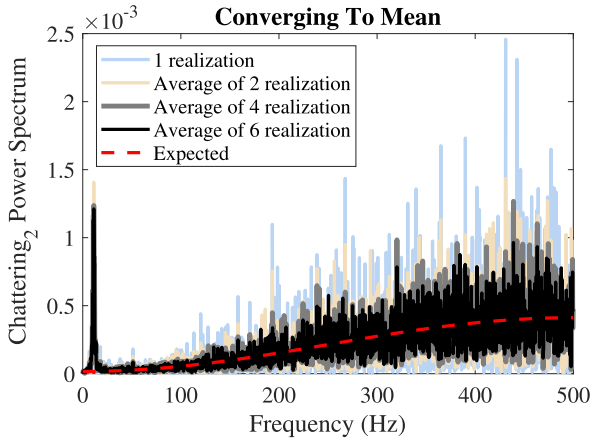

FIGURE 6. Detection of mismatch by averaging over different realizations.

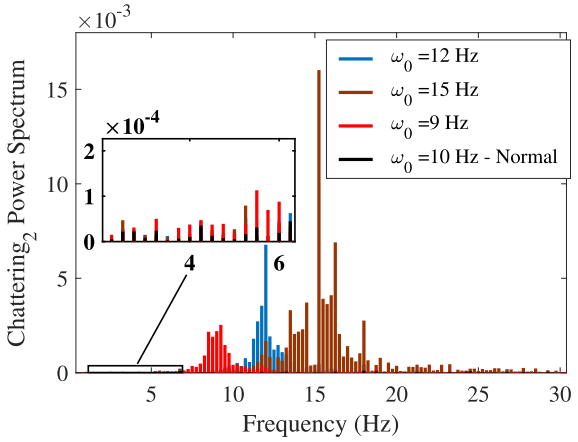

FIGURE 7. Power spectrum of the chattering signal for different levels of mismatch.

shift time is set to be 0.2s (or 0.8s overlap) to have a sharper edge for detecting the start and end of each mismatch period, and the Hamming window function is used as the taper. The spectrogram of the chattering signal is shown in Fig.8 for two input signals: a unit constant function and a step function.

Results accurately pinpoint the frequency and damping mismatches as well as their temporal details. Note that for a constant input, the effect of damping ratio mismatch fades away after a while, because the system stops moving due to damping. However, when the system is excited at $t = 5s$, with the step function input, the impact of the mismatch will become visible in the chattering signal. This shows the importance of persistence excitation especially when a system has a large damping.

In the next section, the proposed method is used for fault detection, and its performance is evaluated.

V. SIMULATION RESULTS FOR FAULT DETECTION IN AN ELECTRO-HYDRAULIC ACTUATOR

The discrete model of the EHA system as described in [32] is used to illustrate the application of the suggested approach for identifying leakage, friction, and bulk modulus mismatch faults. The EHA is a third-order system with state variables that correspond to its position, velocity, and differential pressure, as given in the following state-space model:

TABLE 1. The electro-hydraulic actuator parameters.

Physical Significance	Parameter	Value
Piston Area	A_c	1.52×10^{-3} m^2
Pump Displacement	D_p	5.57×10^{-7} m^3
Mass	M	7.38kg
Leakage Coefficient	L_t	4.8×10^{-12} m^3/s $\cdot$ Pa
Friction Coefficient	a	2144 N$\cdot$ s/m
Bulk Modulus	β_e	2.07×10^8 Pa
System Volume	V_0	1.08×10^{-3} m^3

$$\begin{cases} x_1(k+1) = x_1(k) + T_s x_2(k) + v_1(k), \\ x_2(k+1) = \left(1 - \dfrac{T_s a}{M}\right) x_2(k) + \dfrac{T_s A_c}{M} x_2(k) + v_2(k), \\ x_3(k+1) = \left(1 - \dfrac{T_s \beta_e L_t}{V_0}\right) x_3(k) \\ \quad - \dfrac{T_s \beta_e A_c}{V_0} x_2(k) + \dfrac{T_s \beta_e D_p}{V_0} + v_3(k), \end{cases}$$
$$\begin{cases} z_1(k) = x_1(k) + w_1(k), \\ z_2(k) = x_2(k) + w_2(k), \\ z_3(k) = x_3(k) + w_3(k), \end{cases} \quad (65)$$

where T_s is the sampling time, which is assumed to be 0.001s, $v(k)$ and $w(k)$ are zero-mean white Gaussian noise with the following covariance matrices:

$$\mathbf{v}\mathbf{v}^\intercal = \mathbf{Q} = \text{diag}\left(10^{-12}, 10^{-6}, 1\right)$$
$$\mathbf{w}\mathbf{w}^\intercal = \mathbf{R} = \text{diag}\left(10^{-6}, 10^{-6}, 10^{6}\right) \quad (66)$$

Table.1 provides the nominal values of the parameters in the state-space model (64) [21]. When a leakage fault, friction fault, or bulk modulus mismatch occurs in the system, it causes a change in the associated parameter values L_t, a, or β_e. Following [21], Table.2 summarizes the mismatch scenarios, which are considered to evaluate the ability of the proposed method for handling different levels of defects and faults. This table also shows the corresponding changes in the system's dynamics for each fault regarding damping ratio and natural frequency with respect to their nominal values presented in Table.1.

The system matrices are obtained from (64) as follows:

$$\hat{\mathbf{A}} = \begin{bmatrix} 0 & T_s & 0 \\ 0 & 1 - \frac{T_s a}{m} & \frac{T_s A_c}{m} \\ 0 & \frac{T_s A_c \beta_e}{V_0} & 1 - \frac{T_s \beta_e L_t}{V_0} \end{bmatrix}, \quad \hat{\mathbf{B}} = \begin{bmatrix} 0 \\ 0 \\ \frac{T_s \beta_e D_p}{V_0} \end{bmatrix},$$
$$\hat{\mathbf{C}} = \begin{bmatrix} 1 & 0 & 0 \\ 0 & 1 & 0 \\ 0 & 0 & 1 \end{bmatrix}. \quad (67)$$

Substituting (66) and (67) into (56), (61), and (62), the expected value and the threshold can be calculated for the power spectrum of the chattering signal under normal conditions. An input chirp signal with a frequency ranging

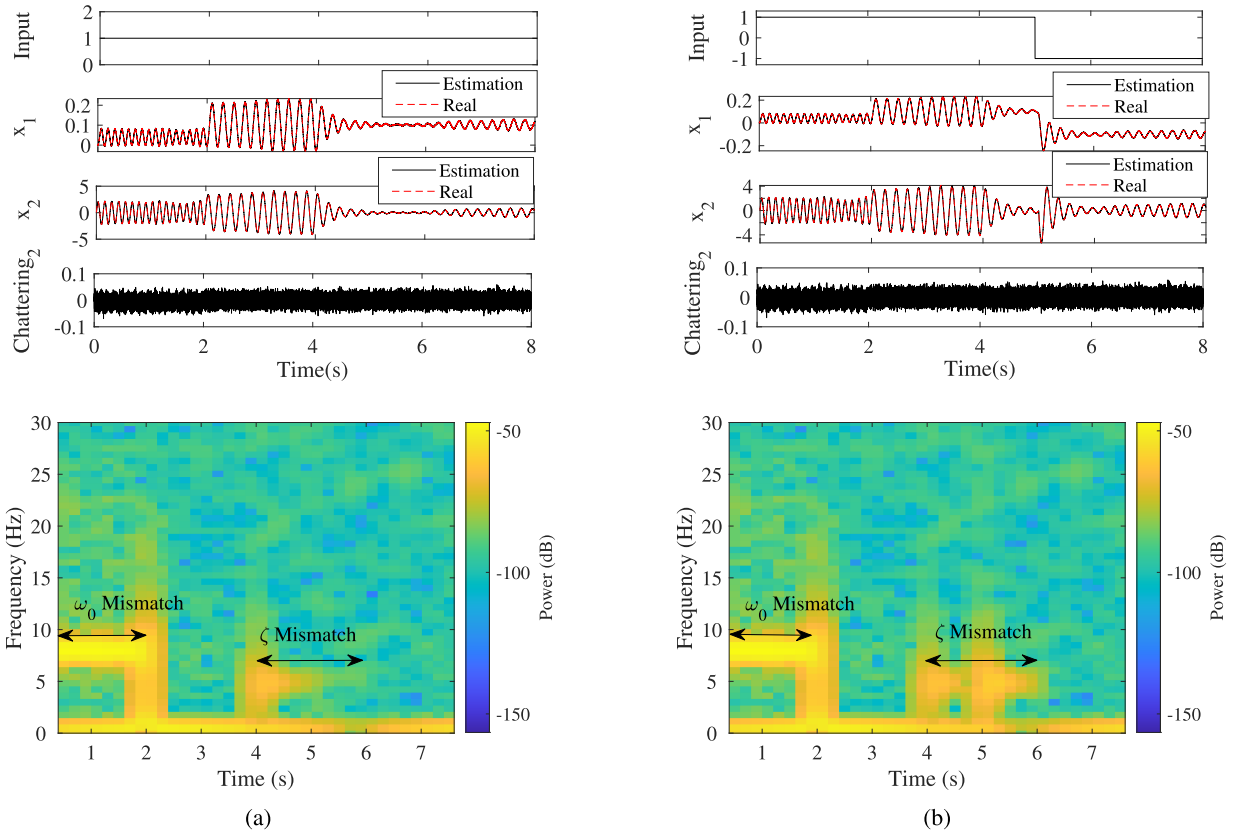

FIGURE 8. Mismatch identification using the spectrogram of the chattering signal for (a) a constant unit input and (b) a step function input.

TABLE 2. Fault levels.

Fault	Level	Affected Parameter	Value	Natural Frequency	Damping Ratio
Healthy	N/A	N/A	N/A	38.9Hz	0.5924
Leakage	Minor	L_t	3×10^{-11} m^3/s · Pa	38.43Hz	0.5895
	Medium		6×10^{-11} m^3/s · Pa	37.88Hz	0.5861
	Major		9×10^{-11} m^3/s · Pa	37.32Hz	0.5826
Friction	Minor	a	4000 N· s/m	38.82Hz	1.1091
	Major		7000 N· s/m	38.7Hz	1.9484
Bulk Modulus	50% down	β_e	$0.5\beta_e$	27.5Hz	0.8392
	25% down		$0.75\beta_e$	33.69Hz	0.6846
	25% up		$1.25\beta_e$	43.49Hz	0.5295
	50% up		$1.5\beta_e$	47.64Hz	0.4830

from 10 to 100Hz is used to excite the system below and above its natural frequency. Fig.9 shows the power spectrum of the chattering signal under the healthy condition. For the error probability $\alpha = 0.1\%$, the power spectrum of the chattering signal follows the expected value trend and remains below the threshold for the corresponding chattering signals of the three state variables. For $\alpha = 1\%$, there are several false alarms in high frequencies, which would be acceptable considering the number of data points ($N = 4000$). However, these false alarms can be avoided by a lower level of α using (64).

Ignoring the negligible impact of the initial error $e_z(0|0)$ in (23), the chattering signal of the EHA for leakage condition is obtained from (67). In this equation, ΔL_t is the mismatch in the leakage coefficient due to leakage fault. As shown in (68), at the bottom of the page 15, leakage fault is observable from the chattering signal of the third state variable that represents differential pressure. Thus, the power spectrum of the pressure chattering signal is used for leakage fault detection. Fig.10 shows that the power spectrum of the chattering signal deviates from the expected value when leakage occurs, with higher leakage levels leading to a larger divergence. However, only major leakage can be detected based on the 0.1% threshold, derived from system noise. This issue can be improved to some extent by deploying a more accurate sensor with a lower level of noise. Additionally, following the idea of Monte Carlo simulation, as shown in Fig.6, the experiment can be repeated, and the average

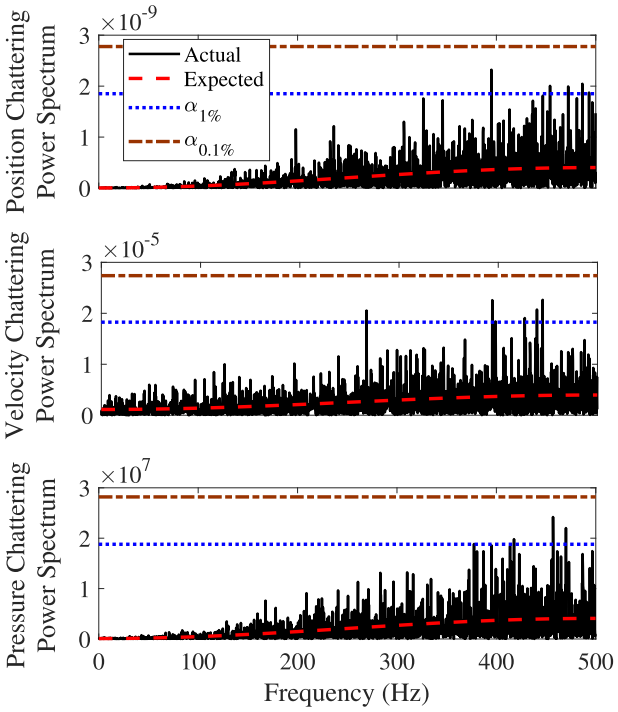

FIGURE 9. Power spectrum of the chattering signal for the EHA system under the healthy condition, where α denotes the error probability.

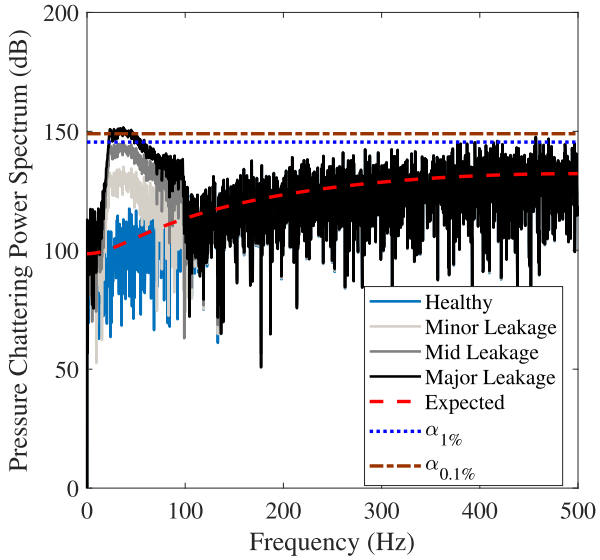

FIGURE 10. Leakage fault detection using spectral analysis of the pressure chattering signal.

of the power spectrum can be calculated. Then, detection can be performed based on the expected power spectrum. As indicated in Table.2, leakage has a small impact on natural frequency. Hence, the power spectrum has a peak at the natural frequency of the system.

Similar to (68), the equation (69), as shown at the bottom of the next page, is used to obtain the chattering signal when there is a friction fault. In this equation, Δa is the mismatch in the friction coefficient due to the fault. The power spectrum

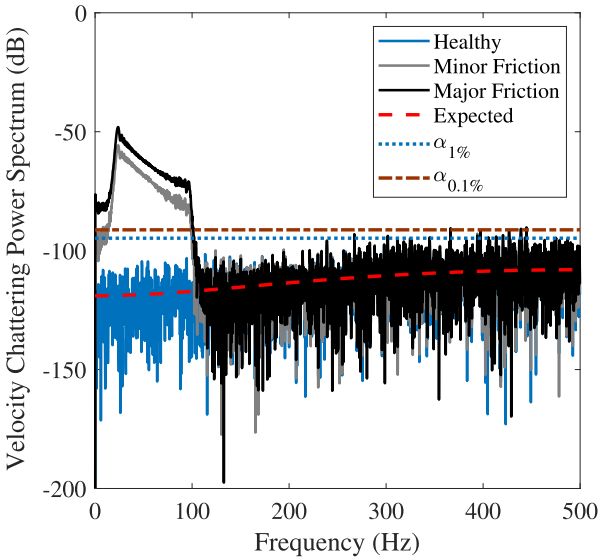

FIGURE 11. Friction fault detection using spectral analysis of the velocity chattering signal.

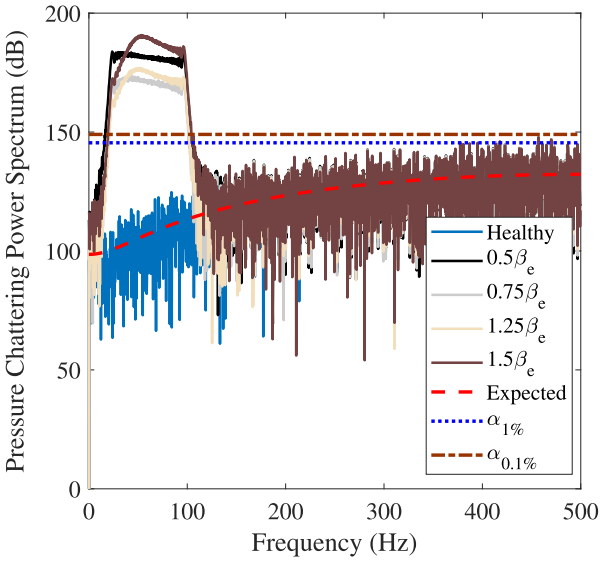

FIGURE 12. Bulk modulus mismatch detection using the spectral analysis of the pressure chattering signal.

of the velocity chattering signal is employed for friction fault identification. As demonstrated in (69), friction fault can be observed from the chattering signal of the second state variable that represents velocity. Fig.11 shows that both minor and major frictions can be detected from spectral analysis. The friction fault has a negligible impact on the natural frequency, but it increases the damping ratio of the system and makes it overdamped (Table.2). The power spectrum does not peak at the natural frequency, because the system becomes overdamped for minor and major friction faults.

The chattering for the bulk modulus mismatch is obtained from (70), as shown at the bottom of the next page. In this equation, $\Delta\beta_e$ is the mismatch in the bulk modulus due to

the fault. The bulk modulus mismatch is detectable from the pressure chattering signal, as indicated in (70). Fig. 12 shows that the bulk modulus mismatch can be identified using the deviation from the expected power spectrum. Furthermore, a larger mismatch leads to a higher degree of deviation. According to Table. 2, a higher bulk modulus increases the natural frequency and decreases the damping ratio of the system. This phenomenon is illustrated in Fig.12.

VI. CONCLUSION

In addition to the innovation vector, which is used in filtering algorithms to correct the predicted state vector in light of the most recent estimation, SVSF benefits from a secondary set of indicators which are the chattering signals associated with different state variables. This paper entertained the idea of using the chattering signal for fault detection and model mismatch identification. In this paper, mathematical expressions were derived for chattering signal of the SVSF for both full-state and partial-state measurement scenarios. Spectrogram of the chattering signal was investigated to extract temporal and spectral information. Building on the idea of Monte Carlo simulation, and taking account of process and measurement noise characteristics, expected value of the chattering signal's power spectrum was obtained under normal conditions. It was proposed to select a threshold for mismatch identification based on a trade-off between avoiding false alarms and minimizing the chance of missing any event that leads to a change in the system under study and causes model mismatch such as fault occurrence. The proposed strategy for choosing this threshold takes the probability distribution of the chattering signal's power spectrum into consideration. A confidence interval is determined using such a distribution that paves the way for fault detection using one realization of the sequence of events, which is suitable for real-time applications. Furthermore, to recover the temporal information regarding a mismatch, the chattering signal can be analyzed using the short-time Fourier transform. The effectiveness of the proposed method for fault detection and mismatch identification was demonstrated through considering a number of scenarios for a typical second-order system and an electro-hydraulic actuator. Furthermore, the proposed framework allows for determining the severity of the mismatch.

Future research can study the implementation of this approach within a closed-loop system for fault diagnosis and development of a Fault Tolerant Control System (FTCS). Considering that the majority of closed-loop systems are designed to demonstrate overdamped dynamics and regarding the fact that the input excitation originates from the controller, addressing challenges in achieving the persistent excitation necessary for fault detection calls for an in-depth exploration.

$$\begin{bmatrix} chattering_1(k+1) \\ chattering_2(k+1) \\ chattering_3(k+1) \end{bmatrix} = \begin{bmatrix} v_1(k) + T_s w_2(k) + w_1(k+1) \\ v_2(k) + \left(1 - \frac{T_s a}{m}\right) w_2(k) + \frac{T_s A_c}{m} w_3(k) + w_2(k+1) \\ \left(1 - \frac{T_s \beta_e \Delta L_t}{V_0}\right) x_3(k) + v_3(k) + \frac{T_s A_c \beta_e}{V_0} w_2(k) + \left(1 - \frac{T_s \beta_e L_t}{V_0}\right) w_3(k) + w_3(k+1) \end{bmatrix}. \tag{68}$$

$$\begin{bmatrix} chattering_1(k+1) \\ chattering_2(k+1) \\ chattering_3(k+1) \end{bmatrix} = \begin{bmatrix} v_1(k) + T_s w_2(k) + w_1(k+1) \\ -\frac{T_s \Delta a}{m} x_2(k) + v_2(k) + \left(1 - \frac{T_s a}{m}\right) w_2(k) + \frac{T_s A_c}{m} w_3(k) + w_2(k+1) \\ v_3(k) + \frac{T_s A_c \beta_e}{V_0} w_2(k) + \left(1 - \frac{T_s \beta_e L_t}{V_0}\right) w_3(k) + w_3(k+1) \end{bmatrix}. \tag{69}$$

$$\begin{bmatrix} chattering_1(k+1) \\ chattering_2(k+1) \\ chattering_3(k+1) \end{bmatrix} = \begin{bmatrix} v_1(k) + T_s w_2(k) + w_1(k+1) \\ v_2(k) + \left(1 - \frac{T_s a}{m}\right) w_2(k) + \frac{T_s A_c}{m} w_3(k) + w_2(k+1) \\ \frac{T_s A_c \Delta \beta_e}{V_0} x_2(k) - \frac{T_s \Delta \beta_e L_t}{V_0} + \frac{T_s \Delta \beta_e D_p}{V_0} u(k) + v_3(k) + \frac{T_s A_c \beta_e}{V_0} w_2(k) + \left(1 - \frac{T_s \beta_e L_t}{V_0}\right) w_3(k) + w_3(k+1) \end{bmatrix}. \tag{70}$$

REFERENCES

[1] Y. Bar-Shalom, X. R. Li, and T. Kirubarajan, *Estimation With Applications to Tracking and Navigation: Theory Algorithms and Software*. Hoboken, NJ, USA: Wiley, 2004.

[2] R. Van Der Merwe, A. Doucet, N. D. Freitas, and E. Wan, "The unscented particle filter," in *Proc. Adv. Neural Inf. Process. Syst.*, vol. 13, 2000, pp. 1–7.

[3] B. Ristic, S. Arulampalam, and N. Gordon, *Beyond the Kalman Filter: Particle Filters for Tracking Applications*. Norwood, MA, USA: Artech House, 2003.

[4] J. S. Liu and R. Chen, "Sequential Monte Carlo methods for dynamic systems," *J. Amer. Stat. Assoc.*, vol. 93, no. 443, pp. 1032–1044, Aug. 1998.

[5] D. Simon, *Optimal State Estimation: Kalman, H Infinity, and Nonlinear Approaches*. Hoboken, NJ, USA: Wiley, 2006.

[6] I. Hwang, S. Kim, Y. Kim, and C. E. Seah, "A survey of fault detection, isolation, and reconfiguration methods," *IEEE Trans. Control Syst. Technol.*, vol. 18, no. 3, pp. 636–653, May 2010.

[7] R. J. Patton and J. Chen, "Robust fault detection using eigenstructure assignment: A tutorial consideration and some new results," in *Proc. 30th IEEE Conf. Decis. Control*, vol. 3, Dec. 1991, pp. 2242–2247.

[8] R. J. Patton and J. Chen, "On eigenstructure assignment for robust fault diagnosis," *Int. J. Robust Nonlinear Control*, vol. 10, no. 14, pp. 1193–1208, 2000.

[9] K. Watanabe and D. M. Himmelblau, "Instrument fault detection in systems with uncertainties," *Int. J. Syst. Sci.*, vol. 13, no. 2, pp. 137–158, Feb. 1982.

[10] J. Wünnenberg and P. Frank, "Sensor fault detection via robust observers," in *System Fault Diagnostics, Reliability and Related Knowledge-Based Approaches*, vol. 1. Rhodes, Greece: Springer, 1987, pp. 147–160.

[11] R. J. Patton and J. Chen, "A review of parity space approaches to fault diagnosis," *IFAC Proc. Volumes*, vol. 24, no. 6, pp. 65–81, Sep. 1991.

[12] J. Gertler, "Fault detection and isolation using parity relations," *Control Eng. Pract.*, vol. 5, no. 5, pp. 653–661, May 1997.

[13] H. Ye, G. Wang, and S. X. Ding, "A new parity space approach for fault detection based on stationary wavelet transform," *IEEE Trans. Autom. Control*, vol. 49, no. 2, pp. 281–287, Feb. 2004.

[14] H. M. Odendaal and T. Jones, "Actuator fault detection and isolation: An optimised parity space approach," *Control Eng. Pract.*, vol. 26, pp. 222–232, May 2014.

[15] P. M. Frank and X. Ding, "Frequency domain approach to optimally robust residual generation and evaluation for model-based fault diagnosis," *Automatica*, vol. 30, no. 5, pp. 789–804, May 1994.

[16] J. Stoustrup and H. H. Niemann, "Fault estimation—A standard problem approach," *Int. J. Robust Nonlinear Control*, vol. 12, no. 8, pp. 649–673, 2002.

[17] R. H. Chen, D. L. Mingori, and J. L. Speyer, "Optimal stochastic fault detection filter," *Automatica*, vol. 39, no. 3, pp. 377–390, Mar. 2003.

[18] R. K. Mehra and J. Peschon, "An innovations approach to fault detection and diagnosis in dynamic systems," *Automatica*, vol. 7, no. 5, pp. 637–640, Sep. 1971.

[19] P. D. Hanlon and P. S. Maybeck, "Characterization of Kalman filter residuals in the presence of mismodeling," *IEEE Trans. Aerosp. Electron. Syst.*, vol. 36, no. 1, pp. 114–131, Jan. 2000.

[20] Y. Chinniah, R. Burton, and S. Habibi, "Failure monitoring in a high performance hydrostatic actuation system using the extended Kalman filter," *Mechatronics*, vol. 16, no. 10, pp. 643–653, Dec. 2006.

[21] S. A. Gadsden, Y. Song, and S. R. Habibi, "Novel model-based estimators for the purposes of fault detection and diagnosis," *IEEE/ASME Trans. Mechatronics*, vol. 18, no. 4, pp. 1237–1249, Aug. 2013.

[22] H. H. Afshari, S. A. Gadsden, and S. R. Habibi, "Robust fault diagnosis of an electro-hydrostatic actuator using the novel dynamic second-order SVSF and IMM strategy," *Int. J. Fluid Power*, vol. 15, no. 3, pp. 181–196, 2014.

[23] P. D. Hanlon and P. S. Maybeck, "Multiple-model adaptive estimation using a residual correlation Kalman filter bank," *IEEE Trans. Aerosp. Electron. Syst.*, vol. 36, no. 2, pp. 393–406, Apr. 2000.

[24] S. Kim, J. Choi, and Y. Kim, "Fault detection and diagnosis of aircraft actuators using fuzzy-tuning IMM filter," *IEEE Trans. Aerosp. Electron. Syst.*, vol. 44, no. 3, pp. 940–952, Jul. 2008.

[25] S. A. Gadsden, S. R. Habibi, and T. Kirubarajan, "A novel interacting multiple model method for nonlinear target tracking," in *Proc. 13th Int. Conf. Inf. Fusion*, Jul. 2010, pp. 1–8.

[26] Q. Zhang, "Adaptive Kalman filter for actuator fault diagnosis," *Automatica*, vol. 93, pp. 333–342, Jul. 2018.

[27] X. Sun, X. Wang, and S. Lin, "Multi-fault diagnosis approach based on updated interacting multiple model for aviation hydraulic actuator," *Information*, vol. 11, no. 9, p. 410, Aug. 2020.

[28] R. Isermann, "Process fault detection based on modeling and estimation methods—A survey," *Automatica*, vol. 20, no. 4, pp. 387–404, Jul. 1984.

[29] R. Isermann, "Supervision, fault-detection and fault-diagnosis methods—An introduction," *Control Eng. Pract.*, vol. 5, no. 5, pp. 639–652, 1997.

[30] E. C. Mid and V. Dua, "Model-based parameter estimation for fault detection using multiparametric programming," *Ind. Eng. Chem. Res.*, vol. 56, no. 28, pp. 8000–8015, Jul. 2017.

[31] V. Stojanovic and D. Prsic, "Robust identification for fault detection in the presence of non-Gaussian noises: Application to hydraulic servo drives," *Nonlinear Dyn.*, vol. 100, no. 3, pp. 2299–2313, May 2020.

[32] A. Saeedzadeh, S. Habibi, and M. Alavi, "A model-based FDD approach for an EHA using updated interactive multiple model SVSF," in *Proc. Fluid Power Syst. Technol.*, vol. 85239. New York, NY, USA: American Society of Mechanical Engineers, 2021, Art. no. V001T01A006.

[33] M. Al-Shabi, S. A. Gadsden, and S. R. Habibi, "Kalman filtering strategies utilizing the chattering effects of the smooth variable structure filter," *Signal Process.*, vol. 93, no. 2, pp. 420–431, Feb. 2013.

[34] L. Ortega, J. Vilà-Valls, E. Chaumette, G. Pagès, and F. Vincent, "Robust tracking under measurement model mismatch via linearly constrained extended Kalman filtering," in *Proc. 59th IEEE Conf. Decis. Control (CDC)*, Dec. 2020, pp. 2924–2929.

[35] S. Habibi and R. Burton, "The variable structure filter," *J. Dyn. Syst., Meas., Control*, vol. 125, no. 3, pp. 287–293, 2003.

[36] S. Habibi, "The smooth variable structure filter," *Proc. IEEE*, vol. 95, no. 5, pp. 1026–1059, May 2007.

[37] S. A. Gadsden and S. R. Habibi, "A new robust filtering strategy for linear systems," *J. Dyn. Syst., Meas., Control*, vol. 135, no. 1, Jan. 2013, Art. no. 014503.

[38] L. H. Koopmans, *The Spectral Analysis of Time Series*. Amsterdam, The Netherlands: Elsevier, 1995.

AHSAN SAEEDZADEH received the B.S. and M.S. degrees in mechanical engineering from the Amirkabir University of Technology, Tehran, Iran, in 2013 and 2016, respectively. He is currently pursuing the Ph.D. degree in mechanical engineering with McMaster University, Hamilton, ON, Canada.

From 2012 to 2016, he was a Research Assistant with the Robotics and Automation Laboratory, New Technology Research Center (NTRC), Tehran. He devoted a period of three years to his role as a Mechanical Engineer within an Iranian start-up enterprise. His research interests include fault detection and diagnosis, state estimation, dynamic control, signal processing, and fluid power control. He was a recipient of the merit-based admission to the Master of Science Program by the Honors Center of Tehran Polytechnic.

PEYMAN SETOODEH (Senior Member, IEEE) received the B.Sc. and M.Sc. degrees (Hons.) in electrical engineering from Shiraz University, and the Ph.D. degree in computational engineering and science from McMaster University. He was a Harrison McCain Visiting Professor with the Marine Additive Manufacturing Centre of Excellence (MAMCE), University of New Brunswick, and an Associate Professor with the School of Electrical and Computer Engineering, Shiraz University. Previously, he was a Senior Research Engineer with the Huawei Noah's Ark Laboratory, and a Lecturer with the Department of Electrical and Computer Engineering, McMaster University, where he is currently with the Centre for Mechatronics and Hybrid Technologies (CMHT). He has coauthored two books: *Fundamentals of Cognitive Radio* and *Nonlinear Filters: Theory and Applications*. He is the coauthor of a paper on "Cognitive Control," which was featured as the cover story of the proceedings of the IEEE in the December issue of the centennial year. His research interests include cognitive systems, artificial intelligence, quantum control, and nonlinear estimation. He was a recipient of the Monbukagakusho Scholarship from the Ministry of Education, Culture, Sports, Science, and Technology, Japan.

MARJAN ALAVI (Senior Member, IEEE) received the B.Sc. degree in electrical engineering (control and instrumentations) from the K. N. Toosi University of Technology, the M.Sc. degree in electrical engineering (micro-and nano-electronic devices) from the Sharif University of Technology, and the Ph.D. degree in electrical engineering from Nanyang Technological University (NTU), Singapore.

In 2015, she joined the Energy Systems Group, Department of Electrical and Computer Engineering, University of Toronto, as a Postdoctoral Fellow. She is currently the Chair of the Manufacturing Engineering Master of Engineering (MEME) Program, W Booth School of Engineering Practice and Technology (SEPT), McMaster University, Canada. She is currently an Assistant Professor with SEPT, teaching in two Bachelor of Technology (B.Tech.) programs; Automation Engineering Technology Program, and Software Technology-Degree Completion Program (DCP). She is also an Associate Member of the Mechanical Engineering and Computer and Electrical Engineering Departments, McMaster University. She is a professional Engineer in ON, Canada. She has several years of industrial experience, as an Electrical Engineer. She has been teaching several courses in electrical engineering at the College and University levels, including digital electronics, embedded systems, the Internet of Things (IoT), artificial intelligence (AI), and smart cities. Her research interests include model-based and data-driven approaches for the diagnosis and prognosis of hybrid systems.

Dr. Alavi was a recipient of the Singapore International Graduate Award (SINGA) 2010. She served on the IEEE Toronto Executive Committee, as the Treasurer, for four years, from 2016 to 2020. She served as the Vice Chair for the IEEE Industrial Applications Society, in 2015, and the Women in Engineering (WIE), from 2018 to 2022. She is the Chair of the Women in Engineering Affinity Group, Hamilton Section, Canada. She was a Reviewer of IEEE TRANSACTIONS ON INDUSTRIAL ELECTRONICS. She is the Guest Editor of *Frontiers in the Internet of Things*.

SAEID HABIBI (Member, IEEE) received the Ph.D. degree in control engineering from the University of Cambridge, U.K., in 1990. He joined McMaster, in 2006, where he was the Chair of the Department of Mechanical Engineering, from 2008 to 2013. In Canada, he was with AlliedSignal Aerospace (presently part of Honeywell), where his last appointment was a Senior Department Manager of Systems Engineering. His extensive technical background includes research into battery modeling and control, state and parameter estimation, mechatronics engineering, fault diagnosis and prognosis, advanced electric drive vehicles, vehicular power and propulsion systems, and energy and sustainability. He has a strong track record of HQP supervision, including 46 master's students and 22 Ph.D., 13 PDFs, and 14 research engineers; many of whom have risen to senior positions in industry, and four have faculty positions. He is currently the Founder and the Director of the Centre for Mechatronics and Hybrid Technologies. He is a full-time Professor with the Department of Mechanical Engineering, McMaster University. He is the Founder and the CEO of EECOMOBILITY Inc., a Canadian start up out of McMaster University, specializing in battery testing and characterization, and AI software and has developed unique test and monitoring products. EECOMOBILITY's products are applicable to batteries, the automotive sector, and electrified powertrains. Also, he has considerable managerial and industrial experience. He spent several years in industry, as a Project Manager and a Senior Consultant of Cambridge Control Ltd., U.K., where he was involved in automotive and aerospace related projects. He received corporate training in both functional and program management. He has more than 200 publications in some of the top journals and three patents. He is a fellow of the American Society of Mechanical Engineers (ASME) and the Canadian Society of Mechanical Engineers (CSME). He was a recipient of several awards. He and his colleagues received the 2012 Best Paper Prize from the IEEE Transportation Electrification Conference for the application of their SVSF theory to condition monitoring of battery cells. He received two corporate awards for his contributions to the AlliedSignal Systems Engineering Process. He was a recipient of the Institution of Electrical Engineers (IEE) F.C. Williams Best Paper Award, for his contribution to the variable structure systems theory. He is the Tier I Canada Research Chair and previously the Senior NSERC Industrial Research Chair (IRC), from 2011 to 2022 (renewed in 2016).